Quaternary uplift on the southeastern coast of Cuba

Christine Authemayou, Leandro Penalver, Denovan Chauveau, Kevin Pedoja, Pedro Dunan Avila, Arelis Nunez, Pedro Benítez Frometa, Edwige Pons Branchu, Alexino Progam, Denyse Martin Izquierdo, et al.

Tectonophysics 910 (2025) 230789

Contents lists available at ScienceDirect

Tectonophysics

journal homepage: www.elsevier.com/locate/tecto

Quaternary uplift on the southeastern coast of Cuba

Christine Authemayou [a,*], Leandro Penalver [b], Denovan Chauveau [a], Kevin Pedoja [c], Pedro Dunan Avila [a], Arelis Nunez [b], Pedro Benítez Frometa [a,b], Edwige Pons Branchu [e], Alexino Progam [e], Denyse Martin Izquierdo [b], Gino de Gelder [d,g], Julie Perrot [a], Ramon Rivada [b], Enrique Diego Arango-Arias [f], Laurent Husson [g]

[a] Geo-Ocean, Univ Brest, CNRS, Ifremer, UMR6538, F-29280 Plouzané, France
[b] Institute of Geology and Paleontology, La Habana, Cuba
[c] Normandie Univ, Unicaen, Unirouen, M2C 1400 Caen, France
[d] Res. Group of Paleoclimate & Paleoenvironment, Res. Centr. for Climate and Atmosphere, Res. Org. of Earth Sciences and Maritime, National Research and Innovation Agency, Bandung, Indonesia
[e] Laboratoire des Sciences du Climat et de L'Environnement, LSCE/IPSL, CEA-CNRS-UVSQ, Université Paris-Saclay, 91191 Gif-sur-Yvette, France
[f] Centro Nacional de Investigaciones Sismológica (CENAIS), Santiago de Cuba, Cuba
[g] ISTerre, CNRS, Université de Grenoble Alpes, Grenoble, France

A B S T R A C T

The southeastern coast of Cuba is bounded on the south by the Oriente Fault Zone that corresponds to the northern Caribbean plate boundary. By analyzing the coastal terraces of this region, we decipher the Quaternary uplift along the transform plate boundary over a ~ 380 km long coastal stretch. We present a detailed mapping of uplifted coastal terraces and 18 new U/Th ages of corals. Late Quaternary uplift rates range from -0.02 ± 0.02 to 0.23 ± 0.07 mm.yr^{-1}. From west to east, the coastal sequences exhibit a maximum of 18 terraces culminating at 270 m on Cabo Cruz, 11 terraces reaching 250 m near Santiago de Cuba and 29 terraces up to 520 m on Punta Maísi. Coastal sequences reveal distinct tectonic regimes. In the west at Cabo Cruz, uplift results from the tilting of tectonic blocks separated by NE-SW-trending normal faults, to the north of an extensional step-over of the Oriente Fault Zone. In the central part, the uplift is associated with NW-SE folding linked to a transpressional relay zone of the Oriente Fault Zone and to the offshore *E*-W Santiago Deformation Belt. In the east, at Punta Maísi, uplift results from a north-dipping thrust close to the coast linked with the oblique collision of the Bahamas platform against Cuba. The intensity of coastal uplift and locations of relay zones seems related to lateral variations in rheology and thickness of the tectonic plates. The uplift of the coast of SE Cuba is controlled by the oblique collision of the Bahamas platform of the North America continental plate against the continental crust of the Caribbean plate to the east and the oceanic/continental transition of the Caribbean plate to the West.

1. Introduction

The northern boundary between the Caribbean plate and the North America plate extends over more than 3000 km, from the subduction of the Cocos plate in the west, to the subduction of the North America plate in the east. In the east, the plate boundary varies from orthogonal subduction in the Lesser Antilles to oblique subduction in Puerto Rico and the Dominican Republic, to pure strike-slip at the Cayman basin (Mann et al., 2002). This latter east-west strike-slip plate boundary zone is made up, in its central part, of two sinistral strike-slip faults, the Oriente Fault Zone (OFZ) to the north, and the Enriquillo-Plantain Garden Fault Zone (EPGFZ) to the south, which frame the Gonave block (Fig. 1). At the western boundary of the block, the Cayman pull-apart oceanic ridge has been open since the Eocene (Donnelly, 1989; Rosencrantz, 1990). At its eastern boundary, the OFZ cuts across the extinct Caribbean island-arc, formed during the Mesozoic subduction of the proto-Caribbean oceanic lithosphere (Mann et al., 1991), which consists of Cuba in the north and the islands of Jamaica, Hispaniola, Puerto Rico and Virgin islands to the south. These characteristics make the Gonave block a complex block with a post-Eocene oceanic nature to the west and an older and thicker crust to the east with an increase of the lithospheric thickness east of Jamaica (Fig. 1). In addition to this lateral contrast in rheology and thickness, the Gonave block boundary is characterized by a purely strike-slip movement in the west, while to the east, it undergoes transpressions produced by the oblique convergence of the Bahamas carbonate platform towards the extinct upper Cretaceous volcanic Caribbean island-arc (Fig. 1).

The aim of this study is to characterize the vertical movements

* Corresponding author.
E-mail address: christine.authemayou@univ-brest.fr (C. Authemayou).

https://doi.org/10.1016/j.tecto.2025.230789
Received 11 June 2024; Received in revised form 2 May 2025; Accepted 16 May 2025
Available online 22 May 2025

produced along the northern boundary of the Gonave block in order to analyze the strain distribution in these laterally contrasting kinematic and crustal settings. More precisely, we investigated the emergent sequences of coastal terraces found along the south east coast of Cuba (southern coast of "Cuba Oriental"). These coastal terraces fingerprint the temporal and spatial variations of Quaternary uplift related to the OFZ on the North America plate side. We mapped the sequences of coastal terraces over a 380-km long coastal stretch, locally on high-resolution Pleiades Digital Elevation Models (DEM) combined with differential Global Positioning System (GPS) measurements and field mapping. We completed the analysis by determining the regional altitudinal variations of the upper coastal terraces with projected topographic parallel staked profiles (swath profiles, Armijo et al., 2015). We dated the lowermost coastal terraces using uranium-series methods on corals and evaluated average uplift rates during the upper Quaternary. We added 18 ages on previously undated sites, including the world-class Cabo Cruz site. Finally, we discuss our results in the framework of the North America/Caribbean plate boundary and try to answer two questions. Do the lateral rheological variations of the southern plate produce variations in the tectonic regime along the plate boundary involving uplift variations of the northern edge of this plate boundary? How does the oblique collision of the Bahamas platform impact the uplift of the northern edge of the Caribbean/North America plate boundary?

2. Setting

2.1. Geodynamics and geology of Cuba

In the northern Caribbean region, Cuba is located on the southern part of the North America plate at its boundary with the Caribbean plate (Fig. 1). Along this plate boundary, the North America plate moves at a rate of 20 mm.yr^{-1} towards the ENE, with a 10–20° obliquity (DeMets et al., 2000; Symithe et al., 2015; Fig. 1). Cuba belongs to an ancient Caribbean island arc, which formed during the Cretaceous (Burke, 1988; Pindell et al., 2012; Hastie et al., 2013; Fig. 1). During the Late Cretaceous-Paleocene, this arc collided with the Bahamas carbonate platform and was subsequently fragmented during the Neogene into several tectonic blocks that crop out today in the Greater and Lesser Antilles (Pindell and Dewey, 1982; Burke, 1988; Mann et al., 1995; Cruz-Orosa et al., 2012; Leroy et al., 2000). In Cuba, the Paleocene-Eocene collision formed a NW-trending orogenic belt (Iturralde-Vinent, 1994; Gordon et al., 1997; Cruz-Orosa et al., 2012). The volcanic arc diachronically collided with the buoyant Bahamas platform from west to east. The direction of convergence between the North America plate and the Caribbean plate changed from SW to W because of this collision (Boschman et al., 2014). During the Oligocene to Miocene in Cuba, left-lateral strike-slip faults (i.e., Pinar, Trocha and Cauto-Nipe faults) progressively relocated the plate boundary southward, fragmenting the Cuban subduction-collision accretionary prism and bounded Neogene post-orogenic basins (Rosencrantz, 1990; Gordon et al., 1997; Iturralde-Vinent and MacPhee, 1999; Leroy et al., 2000; Rojas-Agramonte et al., 2006; Cruz-Orosa et al., 2012; Fig. 1). The western extension of these strike-slip faults opened the Yucatan basin during the Paleocene, and the oceanic Cayman trough during Eocene to Quaternary time (Leroy et al., 1996, 2000; Pablo Ramos and Mann, 2023; Fig. 1). During Oligocene times, the northern boundary of the Caribbean plate shifted to its current position along the Oriente Fault Zone (OFZ) running from the Cayman trough to southern Cuba (Calais and De Lépinay, 1995; Mann, 1997; Calais et al., 2016; Leroy et al., 2000; Pindell et al., 2005; OFZ, Fig. 1). During the Pliocene, the OFZ connected to the Septentrional fault east of Cuba (Oliveira de Sá et al., 2021). Currently, the OFZ, south of Cuba, consists of connected strike-slip faults with transpressional and transtensional step-overs. West of the southeastern coast of Cuba, at Cabo Cruz, the OFZ is associated with a transtensional step-over forming the

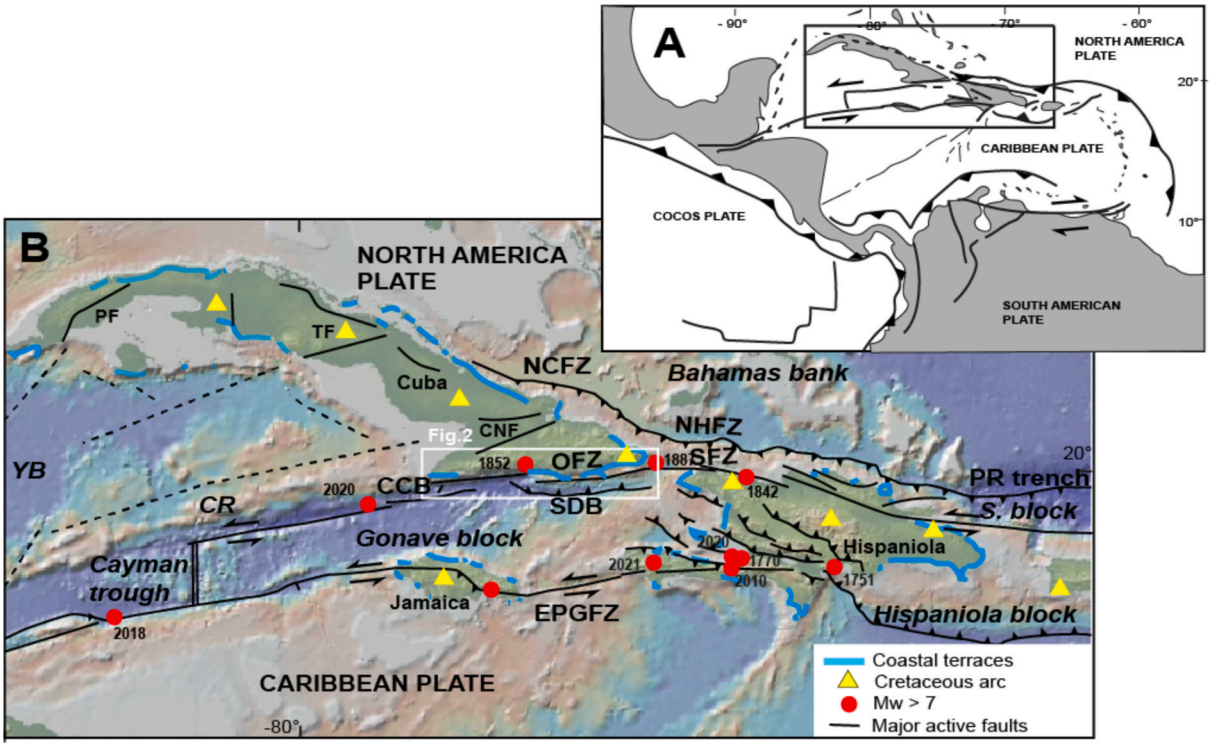

Fig. 1. Geodynamics of the northern Caribbean plate. A: Geodynamic framework. B: Tectonic pattern, location of major earthquakes from USGS/NEIC catalog and coastal terraces (Mann et al., 1995; Pindell et al., 2005; Muhs and Budahn, 2009; Muhs et al., 2017; Viruete and Pérez, 2020; Peñalver et al., 2021; Oliveira de Sá et al., 2021; Calais et al., 2023). PF: Pinar fault, TF: la Trocha Fault, CNF: Caute Nipe Fault, NHFZ: North Hispaniola Fault Zone, NCFZ: North Cuba Fault Zone, CCB: Cabo Cruz Basin, CR: Cayman Ridge, OFZ: Oriente Fault Zone; SFZ: Septentrional Fault Zone; EPGFZ: Enriquillo-Plantain-Garden Fault Zone; S. block: Septentrional block; SDB: Santiago Deformed Belt, PR trench: Puerto Rico trench, YB: Yucatan basin.

Cabo Cruz basin (CCB, Fig. 1). In its central part, to the east of Santiago de Cuba, the OFZ is associated with the Santiago Deformed Belt southward of the OFZ (SDB, Fig. 1).

Along the northern margin of Cuba, the oblique subduction-collision between the Caribbean island arc and the carbonate platform of the Bahamas ended by the suture of the subduction zone (Gordon et al., 1997; Pindell et al., 2005). This structure is currently being reactivated southeastward of Cuba as the western extension of the northern Hispaniola Fault Zone (NCFZ, Fig. 1) named the North Cuban Fault Zone (Oliveira de Sá et al., 2021; Oliveira de Sá, 2023). Since the Late Cenozoic, the collision has progressively uplifted Cuba and Hispaniola (Mann et al., 1991; Calais et al., 1992; Pubellier et al., 2000; Symithe et al., 2015; Wessels, 2019; Escuder-Viruete and Pérez, 2020). At the southeastern tip of Cuba on the Maísi Peninsula, uplift is recorded by the formation of an impressive sequence of coastal terraces that have emerged since the end of Pliocene (Muhs et al., 2017; Peñalver et al., 2021; Authemayou et al., 2023; Fig. 1).

2.2. Sequences of coastal terraces of the southeastern coast of Cuba

Sequences of coastal terraces are widespread along the coasts of Cuba (Peñalver et al., 2021) attracting attention since the end of the 19th century (Crosby, 1883; Agassiz, 1894; Hill, 1895; Vaughan and Spencer, 1902; del Corral, 1944; Núñez Jiménez, 1973; Busto del Busto, 1975; Horsfield, 1975). Most terraces are constructional reefs but erosional marine benches have truncated some of these. The most ubiquitous is the terrace from the peak of last interglacial (Marine Isotope Stage (MIS) 5e, ~120 ka, Peñalver et al., 2021). Its associated deposits and bio-constructions are locally described as the Jaimanitas formation (Rojas-Agramonte et al., 2005; Toscano et al., 1999; Iturralde-Vinent, 2003; Iturralde-Vinent, 2009; Muhs et al., 2017; Peñalver et al., 2003, 2021).

Near Cabo Cruz, the southwestern tip of Cuba main island, Taber (1934) described a sequence of 12 successive terraces (Figs. 1, 2). The same author, taking into account the maximum elevation of the sequence (270 m), privileged a Quaternary coastal uplift over eustatic sea level variations as responsible for the emersion of the sequence. In the central stretch of the southeastern coast, Rojas-Agramonte et al. (2005) revealed the tectonic uplift of the Santiago de Cuba area from a sequence including four terraces up to ~200 m in elevation. In the Guantanamo Bay area, Meinzer (1933) recognized the low-elevation terrace formed by the Jaimanitas formation. Analyzing these coastal terraces, estimates of paleo-sea level during MIS 5e (6 to 11 m) and U/Th ages (~125 ka to ~115 ka), Muhs et al. (2017) estimated late Quaternary uplift rates to 0.02–0.11 mm.yr^{-1} for the southern zone of Guantanamo Bay (Fig. 2). Terrace sequences are best developed at Punta de Maísi, on the southeastern tip of Cuba, both in terms of the extent and number of successive terraces (del Corral, 1944; Busto del Busto, 1975; Horsfield, 1975; Peñalver et al., 2003, 2021; Muhs et al., 2017; Authemayou et al., 2023). On the southern side of Punta de Maísi, the sequence exhibits 29 coastal terraces up to 520 m in elevation and an apparent Quaternary uplift rate of 0.23 ± 0.07 mm.yr^{-1} (Authemayou et al., 2023). Horsfield (1975), based on the number of successive terraces, proposed a higher uplift rate to the east (Punta de Maísi) compared to the west (Cabo Cruz).

3. Methods

3.1. Mapping coastal terrace sequences

In tropical zones, the staircase morphology of a coastal terrace sequence is the result of the interactions between reef accretion (bio-construction and sedimentation), relative sea level changes, erosion (marine and continental) and the initial coastal geomorphology (Camoin and Webster, 2015; Husson et al., 2018; Chauveau et al., 2021), resulting in a wide spectrum of morphologies (Pedoja et al., 2018). Notably, in addition to bioconstruction, marine erosion and the resulting sedimentation can "smooth" the inner part of the reef and cause the sea cliff to retreat (e.g., Pastier et al., 2019; Chauveau et al., 2024a, 2024b). The inner edge (map view) and associated shoreline angle (profile view) of coastal terraces correspond to the junction of a wave-cut bench with the sea cliff landward of the bench (Davis, 1933; Lajoie, 1986; Pedoja et al., 2011, 2014).

We mapped the inner edge of coastal terraces using a high-resolution (2 m) DEM (Pleiades). From a range of datasets (hillshades, slope maps, satellite ortho-images, and field data), we contoured the inner edges of each surface corresponding to the base of fossil cliffs landward of modern sea level. Lateral correlation of coastal terraces across valleys is based on the continuity of elevations, platform width, and equivalent position in the coastal terrace sequence. In order to get precise elevations, we acquired topographic profiles using a kinematic differential global positioning system (RTK dGPS) (Fig. 2). Our profiles were measured perpendicular to the coastline from present mean sea level. The roughness of the coastal terraces and continental slope deposits at the base of the fossil cliffs are the main source of error in elevation, far beyond real kinematic differential GPS instrumental errors. On T1, the terrace roughness or the slope deposits are less than one meter vertically. Consequently, we assigned an elevation uncertainty of 1 m for all

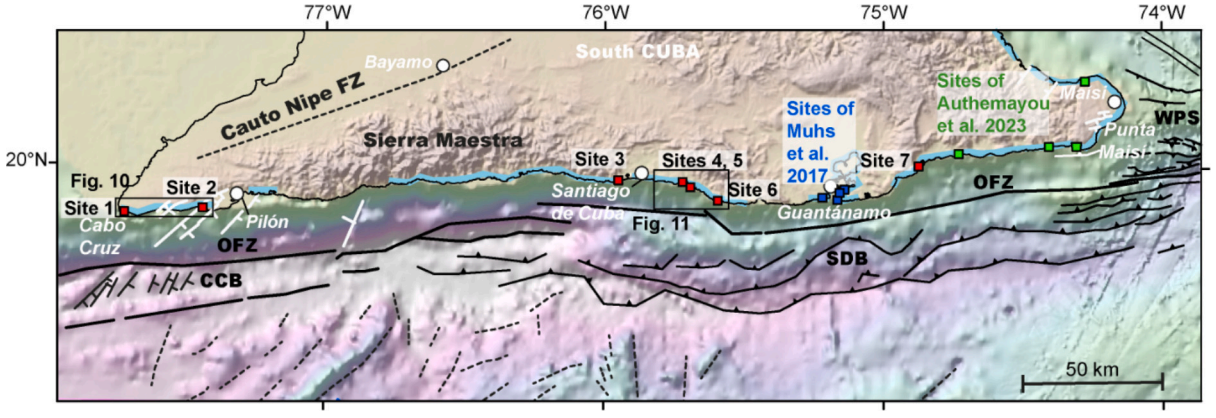

Fig. 2. Tectonic structure and coastal terraces of South East Cuba. Red, blue, green squares are respectively from the current study, from Muhs et al. (2017) and from Authemayou et al. (2023). Blue stretches are emerged coastal terrace sequences (Peñalver et al., 2021). Faults in black are from previous studies (Calais and Mercier de Lépinay, 1991; Leroy et al., 1996; 2015; Corbeau et al., 2016). Faults in white are from this study and from Authemayou et al., 2023.Continuous and dashed lines are active and inferred active faults, respectively. Caute Nipe FZ: Caute Nipe Fault Zone, CCB: Cabo Cruz Basin, OFZ: Oriente Fault Zone; SDB: Santiago Deformed Belt, WPS: Windward Passage Sill.

field estimates except for the site at Verraco. For Verraco, we were unable to take measurements using a differential GPS. We performed a topographical profile using the 2 m high-resolution DEM. The uncertainty in the topographical values is therefore greater than values obtained with differential GPS measurements. Differential GPS data compared with DEM data at the other sites where we have both types of measurement yields an overall uncertainty on the order of 1–2 m. Taking into account this methodological uncertainty, we set an elevation uncertainty of ±2 m for Verraco site.

For two areas (Cabo Cruz zone and Santiago de Cuba zone), we stacked hundreds of parallel topographic swaths from the DEM together (Armijo et al., 2015; de Gelder et al., 2022, 2023; Authemayou et al., 2023; Fig. 2). The elevation of their inner edges was mapped onto these stacked swath profiles, in order to show their cumulative deformation. Distortion of the terraces would depend on the viewing angle with respect to the dip of the terraces. A view perpendicular to the tilt will show horizontal terraces. The correlation of the terraces on the projected profiles is only carried out on the principle of spatial continuity. Put another way, when the terraces are very discontinuous, the major criterion is not to produce abrupt vertical offsets without the presence of a faulted topographic escarpment detected on the DEM. Thus, these correlations remain open to interpretation.

3.2. Sampling strategy and U/Th dating

We focused on seven coastal sites along the southeastern shore of Cuba Island (Fig. 2). We extracted 18 coral samples for U/Th dating, by drilling coral colonies in growth position from the surface of the lowermost coral reef terrace. Low terraces were sampled to minimize the risk of sampling recrystallized coral (from aragonite to calcite) that would prevent reliable dating (Thurber et al., 1965; Bar-Matthews et al., 1993). Indeed, fossil corals can be affected by diagenesis, resulting in age bias. After terrace emergence, aragonite to calcite transformation is one of the main processes affecting fossil coral skeletons. This process results in uranium lossand older apparent ages (Thurber et al., 1965; Bar-Matthews et al., 1993), although it may have a limited effect on the uranium isotopic composition (Thompson et al., 2003). We proceeded with U/Th dating on samples with a majority of aragonite. Thompson et al. (2003) suggest that ages from samples with more than 10 % calcite should be excluded in the analysis.

Other diagenetic alteration can be due to dissolution / recrystallisation processes, with incorporation or loss of uranium and thorium, but also in some cases by the precipitation of secondary aragonite. These alterations could also cause age bias that can be identified by isotopic uranium signature not compatible with the marine one, by mineralogical determination, by thin section analysis (e.g. Hamelin et al., 1991, Thompson et al., 2003 and review in Ribot et al., 2024). In our study, the validation of $^{230}Th/^{234}U$ ages has been done by comparison of the initial ratio between ^{238}U and ^{234}U (expressed as $\delta^{234}Uo$ of the coral with the modern seawater (msw) uranium isotopic composition, i.e., $\delta^{234}U(msw) = 145.5 \pm 2.3$ ‰; Cheng et al., 2000, $\delta^{234}U(msw) = 145 \pm 1.5$ ‰; Chutcharavan et al., 2018). The difference between calculated $\delta^{234}U_o$ and msw of 5 ‰ higher or lower is considered a sign of diagenetic alteration (Chutcharavan et al., 2018), and a further correction is applied. We use the model provided by Thompson et al. (2003) for these samples to determine an open system age (Supplementary Table 1).

The samples were mechanically cleaned with a micro-drill, rinsed in MilliQ water, and leached in chloridric acid dilute (0.1 N) bi-distilled HCl for 15–20 min in an ultrasonic bath. The cleaned samples (large pieces of coral) were then crushed into powder and analyzed using XRD Brucker D8 at the LCG (Laboratoire d'étude des "Cycles Géochimiques et Ressources", IFREMER) in Brest (France) to quantify the relative quantities of calcite and aragonite. Subsequently, the powders were covered with milliQ water and dissolved by adding drops of concentrated HCl, in beakers where a known amount of a mixed ^{229}Th-^{233}U-^{236}U spike previously was added to the solution. After co-precipitation with FeOH, the uranium and thorium fractions were purified using U-TEVA resin in nitric media, following a procedure modified from Pons-Branchu et al. (2005). Thorium and uranium fractions were recovered using HCl 3 N and 1 N respectively.

In order to support our method, we carried out replicate analyses by taking samples directly from the pieces of coral using a micro-drill (see photo and table in supplementary data), without prior acid cleaning of sample. For these analyses, we selected Cub 19–31, which is not likely to have been affected by diagenesis (initial $\delta^{234}U_o$ of 143.8 ± 1.2 and 99 % aragonite, Supplementary Table 1). The results are presented in supplementary data. The results obtained without leaching of the sample with dilute HCL (Cub 19–31-a, b and c) show in all 3 cases fairly low uranium contents (below 2 ppm), without showing any variation in the calculated age. The protocol used does not therefore result in any visible fractionation between uranium and thorium and therefore no bias in the age. The small variations in U content could be due to heterogeneities in the structure of the coral (vital centres), which have been widely documented for tropical corals.

The uranium and thorium isotopic compositions were analyzed on a Multi-Collector Inductively Coupled Plasma source Mass Spectrometer (MC-ICPMS) Thermo ScientificTM NeptunePlus fitted with a jet pump interface and a dissolving introduction system (aridus II). For mass fractionation correction, we used an exponential law (normalized to natural $^{238}U/^{235}U$ isotopic ratio) and standard/sample bracketing. More details on the analytical procedure (chemistry and MC-ICPMS analysis) can be found in Pons-Branchu et al. (2022). After corrections for peak tailing, hydrate interference and chemical blanks, $^{230}Th/^{234}U$ ages were calculated from measured atomic ratios through iterative age estimation using the ^{230}Th, ^{234}U and ^{238}U decay constants of Jaffey et al. (1971) and Cheng et al. (2013).

3.3. Sequences of coastal terraces and uplift rates

Sequences of coastal terraces make it possible to estimate the rates of late Quaternary coastal vertical motion. Uplift rates are calculated from shoreline angle elevation, terrace age and paleo-sea level at the time of terrace formation (e.g., Murray-Wallace and Woodroffe, 2014; Pedoja et al., 2014; Rovere et al., 2016). Although the relationship is not always straightforward, the shoreline angle generally marks mean sea level at the time of terrace formation(Lajoie, 1986). In practice, the age of corals in growth position on the upper part of the coastal terrace help to determine the highstand responsible for the final formation of the coastal terrace. The depth at which coral grows can vary greatly (0 to 20 m for *Dichocoenia stokesii*; Aronson et al., 2008, Supplementary Table 1). To reconstruct the uplift rates, we used the elevation of the shoreline angle (i.e., the inner edge of the terrace), corresponding to the maximum sea level at the highstand (e.g., Murray-Wallace and Woodroffe, 2014; Pedoja et al., 2014; Rovere et al., 2016, 2022).

The most commonly preserved interglacial period worldwide in the geomorphological record is MIS 5 (Stirling et al., 1998; Pedoja et al., 2011, 2014; Murray-Wallace and Woodroffe, 2014; Rovere et al., 2016, 2022; Creveling et al., 2017; Barlow et al., 2018; de Gelder et al., 2022; Weiss et al., 2022. Hsia et al., 2024; Fouke and Kerans, 2024). MIS 5 includes three relative highstands, MIS 5a (~ 80 ka), MIS 5c (~100 ka) and MIS 5e (~120 ka). Hsia et al., 2024 estimated an MIS 5a global mean sea level highstand of −6.5 to −5.1 m and Muhs et al. (2011) estimated an MIS 5e of 2 to 8 m eustatic highstand for the Florida region using dated corals from cores and from fossil reefs outcrops.

4. Results

The lowermost terraces of the southeastern part of Cuba are found almost continuously along the coast except for a 45 km segment of coastline along the Sierra Maestra massif (west of Santiago of Cuba) (Fig. 2). In the study area, we focused on 7 sites which correspond to the best-preserved and most-complete (in terms of number of successive

terraces) coastal sequences, with the exception of the sequences of Punta de Maísi which were recently dated and described in detail elsewhere (Authemayou et al., 2023).

4.1. Site 1: Cabo Cruz

At the western end of the southeastern coast of Cuba (Cabo Cruz), we observed a sequence of two coastal terraces (T1 and T2) with T2 having a maximum elevation of 24 m above present mean sea level (apmsl) (Figs. 2 and 3). We surveyed the lowermost coastal terrace (T1) and the dGPS profile shows that its inner edge lies at an elevation of 2.6 ± 1 m (Fig. 3B). The surface of T1 slopes seaward with its distal part eroded near modern sea level (Fig. 3C). Boulders derived from the upper terrace partially cover this surface. T1 is composed of a maximum 2.5 m thick reefal units including corals in growth position. We sampled and U/Th dated two corals in growth position from the T1 reef unit (Figs. 3B, C, D, Supplementary Table 1). Samples CUB19.34 and CUB19.35 yielded ages of 119.6 ± 1 ka and 119.8 ± 1 ka, respectively (Fig. 3B, Supplementary Table 1).

4.2. Site 2: Boca del Toro

At Boca del Toro, 27 km east of the site 1 (Cabo Cruz), we identified a sequence of at least four coastal terraces (Figs. 2 and 4 A). Westward, the sequence is more complete and includes seven terraces (Fig. 4B). The coastal terraces T1 and T3 are narrower than the coastal terraces T2 and T4 (Fig. 4A). The T1 inner edge is found at an elevation of 8 ± 1 m on the dGPS profile (Figs. 4C, D). The distal edge of the terrace is at 5 m ± 1 m. Six samples (CUB19.26 to CUB19.31) in growth position were drilled in coral colonies found on the surface of the terrace, close to its distal edge. They yielded ages of 79.8 ± 0.5 ka to 85.4 ± 0.3 ka (Figs. 4A, E, Supplementary Table 1). One sample CUB19.25, taken next to the samples CUB19.27, 19.28, 19.26, provided an age of 132.9 ± 1 ka (Fig. 4A, Supplementary Table 1).

4.3. Site 3: Rancho Cruz

14 km southwest of Santiago de Cuba, we observed two terraces (Figs. 2 and 5 A). On the dGPS profiles, the inner edge of the lower terrace (T1) was measured at 7 ± 1 m and its distal edge at 4 ± 1 m (Fig. 5B). A topographic step of 1 m height is visible in the central part of the lower marine terrace. T1 inner edge is associated with a well-preserved notch (Figs. 5C and D). A coral in growth position (CUB22.64 on T1) sampled at the central part of the terrace upper surface, yielded a U/Th age of 134.4 ± 1 ka (Figs. 5B, E and Supplementary Table 1).

4.4. Site 4: Western Siboney

At the Western Siboney site, 14 km southeast of Santiago de Cuba, we observed a sequence of five terraces (Figs. 2 and 6A). The lowermost terrace (T1) is the widest. Its sinuous distal edge bears witness to the efficiency of marine erosion (Fig. 6B). On the dGPS profile, the inner edge of T1 is at 8 ± 1 m and the distal edge is at 4 ± 1 m (Fig. 5B). The dGPS profile defines an intermediate scarp of 2 m height located ~150 m landward of the modern shore (Fig. 5C). Corals in growth position in the middle and in the distal edge of the terrace,CUB19.08, 19.09, 19.13, were dated to 130.6 ± 0.9 ka, 129.7 ± 0.9 ka and 140.4 ± 0.9 ka respectively (Figs. 6C, D and Supplementary Table 1).

4.5. Site 5: Bucanero

Site 5 at Bucanero is 3 km east of site 4 and the sequence includes three terraces (Figs. 2 and 7A). The lowermost and widest (200–250 m)

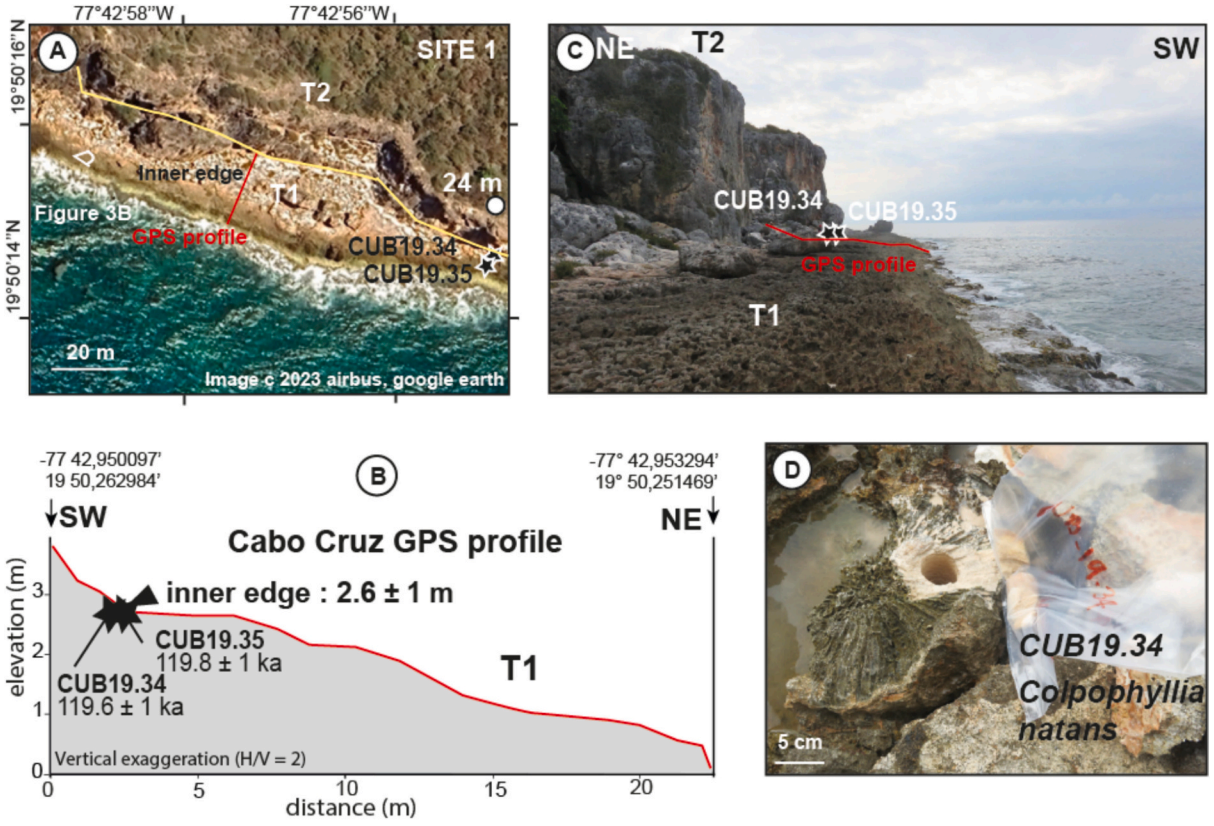

Fig. 3. The coastal sequence at Cabo Cruz site (site 1 of Fig. 2). A) general view from satellite imagery with samples and dGPS locations, B) dGPS profile and sampling locations. C) and D) Interpreted field pictures and sampling details.

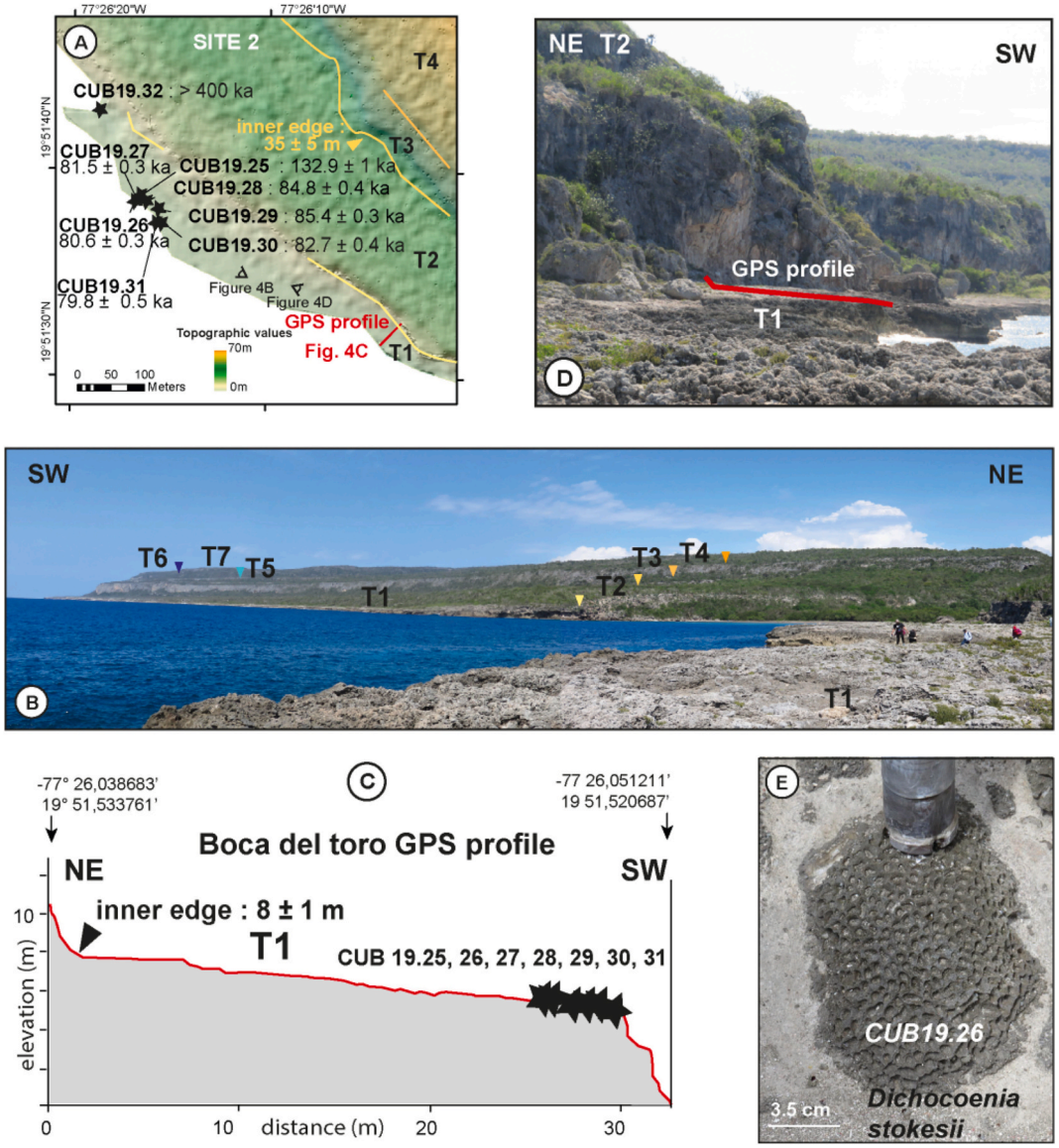

Fig. 4. The coastal sequence at Boca del Toro site (site 2 of Fig. 2). A) general view from satellite imagery with sample ages and GPS location, B) Interpreted picture of coastal sequence view from Boca del Toro site. C) dGPS profile and sampling locations. D), E) Interpreted field pictures.

terrace (T1) provided the foundation of the Bucanero hotel complex, which was destroyed by hurricane Sandy in 2012 (see Pedoja et al., 2023). On the dGPS profile, the inner edge of T1 is found at 9.5 ± 1 m and its distal edge is at 4.5 ± 1 m (Figs. 7B, D). We sampled four corals in growth position on the surface of T1. U/Th dating of 19.17 next to the dGPS profile yield age of 136.5 ± 0.8 ka (Fig. 7A, Supplementary Table 1). CUB 22.55, CUB 22.56, 22.57, 300 m westward of the dGPS profile, yielded ages of 112.9 ± 0.5 ka, 132 ± 0.7 ka, and 119.7 ± 0.6 ka, respectively (Fig. 7A, Supplementary Table 1).

4.6. Site 6: Verraco

At a locality 32 km southeast of Santiago de Cuba, we observed two terraces (Figs. 2 and 8 A). The lowermost (T1) is wider (350 m) and higher (~35 m) compared with the T1 terraces of the other sites described above (from 30 to 250 m wide and from 1.6 to 10.5 m high).

Topographic profile extracted from Pleiades DEM shows its inner edge at an elevation of 35 ± 2 m (Figs. 8 A and 8B). The active cliff in the distal edge rises 12 m above sea level (Fig. 8C). As the vegetation was denser than on the other sites, we were unable to find well-preserved corals for dating.

4.7. Site 7: Bate Bate

37 km southeast of Guantanamo Bay, at Bate Bate, a sequence includes five terraces (Figs. 2 and 9A). The lowermost terrace (T1) is wide (220 m). Its distal part is devoid of vegetation and is partly covered by what we interpret to be storm deposit ~40 m from the seaward edge (Figs. 9A and B). On the dPGS profile, the T1 inner edge is at 11 ± 1 m and the distal edge is at 6 ± 1 m above sea level (Fig. 9C). We sampled two corals in growth position at the top of the surface. CUB22.48 and CUB 22.49 yielded U/Th ages of 121.5 ± 0.5 ka and 122.9 ± 0.8 ka, respectively (Figs. 9B,C, Supplementary Table 1).

5. Discussion

5.1. Deformation of the coastal terrace sequences

We assembled stacked swath profiles of the topography on two areas of the SE coast of Cuba to complement the stacked swath profiles on the

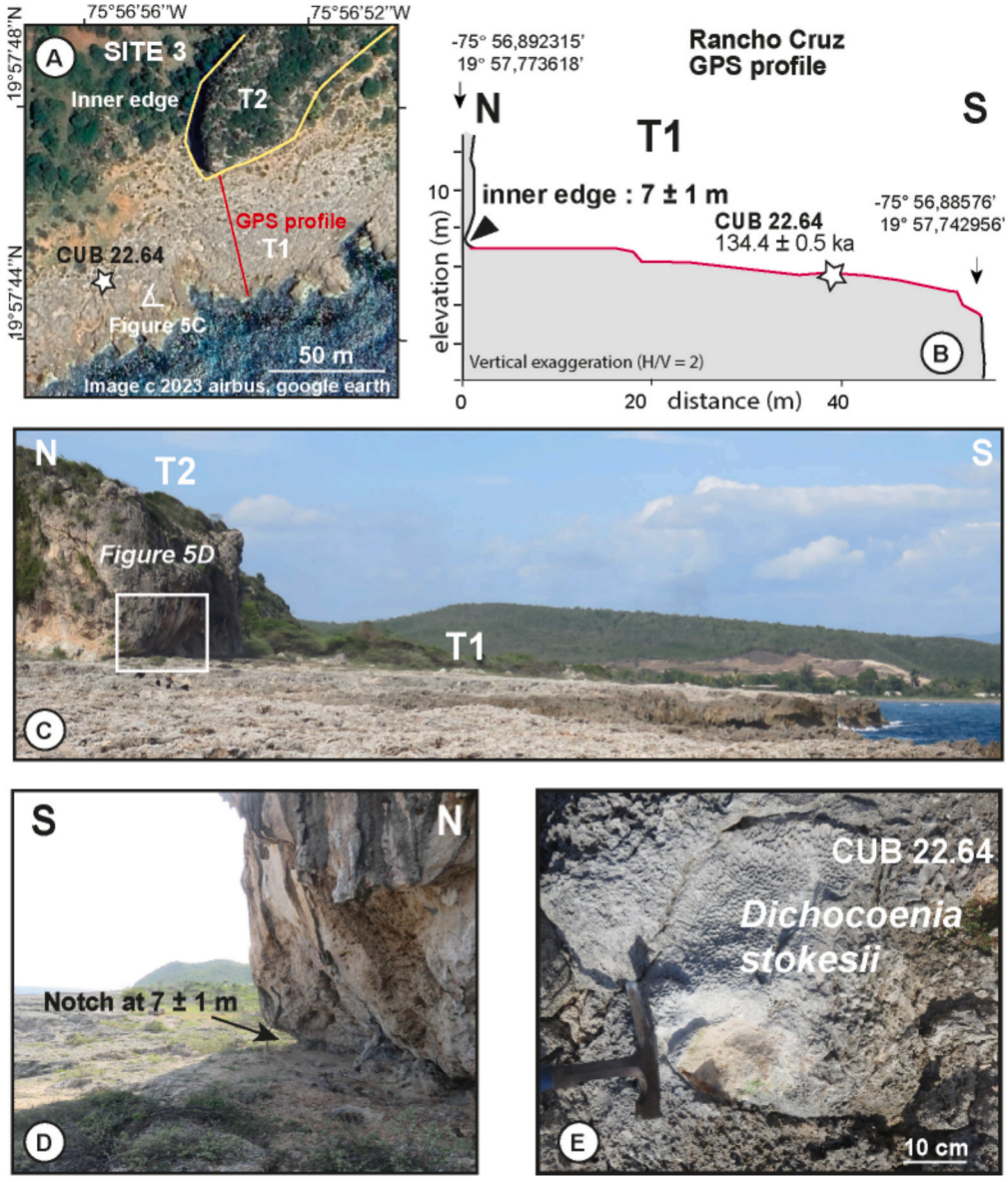

Fig. 5. The coastal sequence at Rancho Cruz site (site 3 of Fig. 2). A) general view from satellite imagery with samples and GPS locations, B) GPS profile and sampling locations. C), D) and E) Interpreted field pictures and sampling details.

eastern tip of this coast (Authemayou et al., 2023, Figs. 2, 10, 11). These profiles illustrate spatial variations in the amount of uplift and in particular in the key sites along the transform fault (OFZ, Fig. 2). The western zone in Cabo Cruz (Fig. 10) shows a sequence of coastal terraces whose number increases towards the east together with an apparent westward long-wavelength tilt of the inner edges (Figs. 10B, C). The maximum number of detected terraces is 17 to the east, and only 3 to the west. The long-wavelength tilt angle decreases progressively with the terrace level in the sequence. This differential uplift and this evolution are consistent with a progressive deformation of the terraces from the emergence of the sequence until present-day. The topographic stacked swath profiles of Fig. 10D and E show the coastal terraces on a NE-SW-trending section. The terraces are horizontal. Consequently, both E-W and NE-SW projections allow interpretation of a possible tilting of the terraces towards the NW (Fig. 10F). The maximum tilting value of the older terrace is 2° (Fig. 10F). The terraces are sometimes vertically offset by minor faults that produce multi-metric NE-SW-striking escarpments in the topography, indicating the direction of the fault plane (Figs. 10A, G, H). The general tilt of the inner edges which may be related to the vertical component of a NE-SW-striking normal fault, 68 km eastward to the site 2 (bold red line in Fig. 10A). Locally, to the east of the fault and west of Pilón city (Fig. 2), we did not observe any sequence of coastal terraces, with the possibility that the block to the east of this fault is subsiding.

In the central part of the southeastern Cuban coast, to the southeast of Santiago de Cuba, stacked topographic swath profiles show the E-W trending projection of a sequence of coastal terraces (Figs. 11A, B, C, D). The sequence is well marked, with a maximum of 14 identified terraces. For each terrace, the elevation of the inner edge varies longitudinally along the 25 km of coastline. Overall, this elevation increases towards the east, reaching the highest topographic heights in the vicinity of site 6 at Verraco, the most SE point of the studied coastline. This lateral variation is not represented by a long tilt similar to the western coast of Cabo Cruz (Fig. 10). Near site 4 at Western Siboney, the terraces show km-scale asymmetrical folding (Figs. 11B, D). Two anticlines affect the highest terraces, and an anticline affects the intermediate terraces (Fig. 11D). The asymmetry of the folds suggests an apparent west-verging fold system. In the central part of the swath profiles, along the

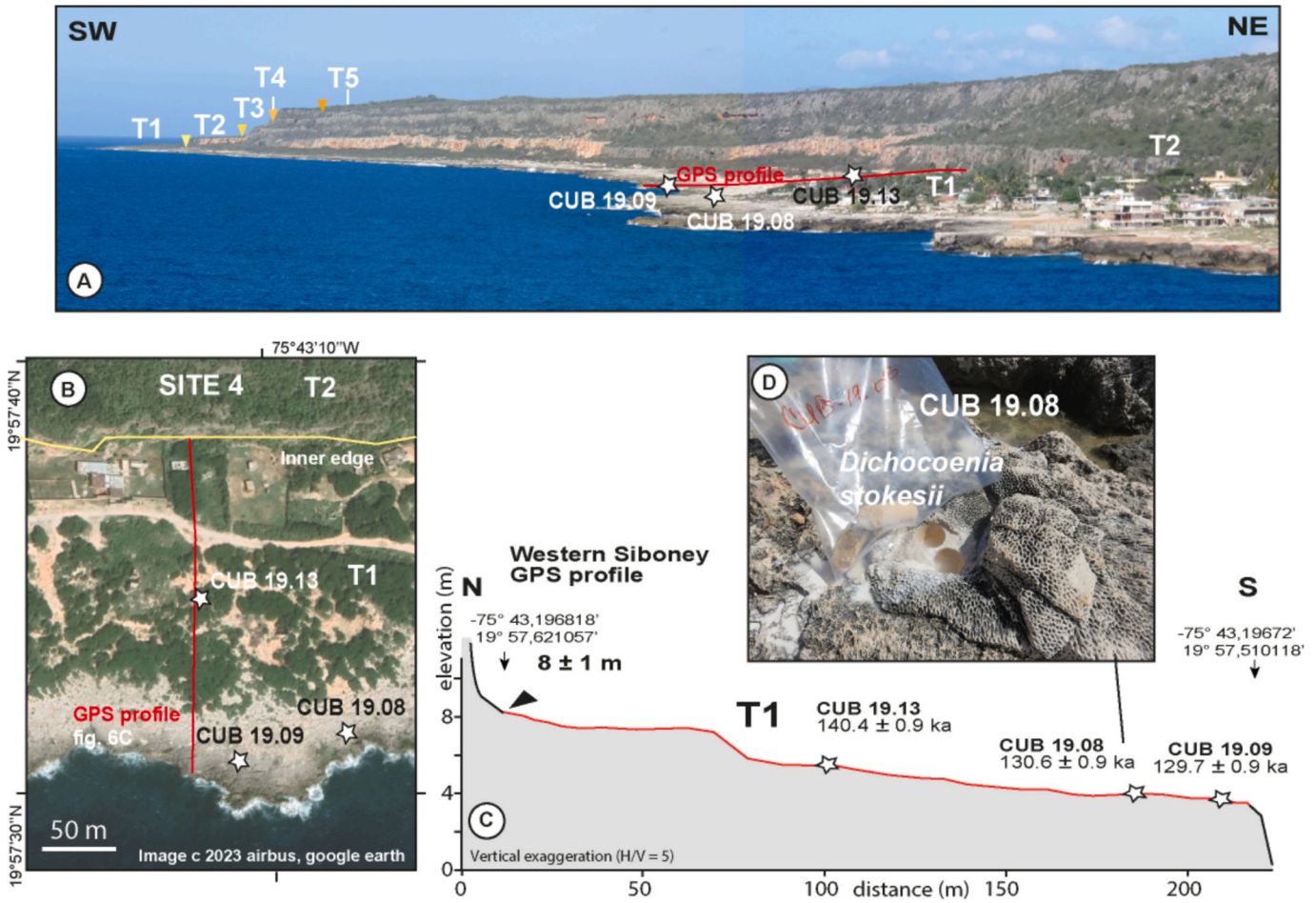

Fig. 6. The coastal sequence at Western Siboney (site 4 of Fig. 2). A) Interpreted picture of the coastal sequence at Western Siboney. B) General view from satellite imagery with samples and GPS locations, C) GPS profile and sampling locations. D) Sampling details.

NW-SE-trending coast, the respective elevations of the coastal terraces do not vary (Fig. 11D). It increases again towards the east when the coastline resumes to its E-W direction (Figs. 11C, D), then remains fixed when the coastline turns NW-SE again (Figs. 11E, F). This sudden increase of terraces elevation when the coast has an E-W direction could be associated with folding too. This folding is better expressed by the highest terraces compared to the lowest terraces, suggesting that folding has been a slow, but ongoing process. As the fold flank tilting on the coastal terraces and the elevation of the central hinge zone of the fold is only visible on the EW-trending coastal sections and not apparent on the NW-SE coastal sections, the axis of the folds is probably NW-SE. This fold axis direction reveals NE-SW shortening, in agreement with an E-W trending sinistral transpressive regime and a NE-SW trending maximum horizontal compressive stress close to the E-W striking fault segment of the Oriente Fault Zone (Moreno et al., 2002).

5.2. Age of the lowermost coastal terraces

At site 1 (Cabo Cruz site), the two U/Th dated corals on the lowermost terrace (T1) yielded an age of ~119 ka corresponding to the MIS 5e sea level peak (~120 ka, Supplementary Table 1). For site 2 (Boca del Toro), one coral (CUB 19.25) sampled from the upper surface of the lowermost terrace (T1) yielded an age of 133 ka, corresponding to the end of the MIS 5e transgression. The other coral samples (CUB 19.26, 27, 28, 29, 30, 31), yielded ages that can be correlated to MIS 5a (~80 ka) (Supplementary Table 1). These ages could correspond to the timing of the construction of the ultimate reef unit construction, during MIS 5a sea level peak (~80 ka). The coral sample CUB19.25 dated at 133 ka is located at the same altitudinal position as MIS 5a coral samples. Because the sea level at 133 ka was already as high as the MIS 5a sea level (Hsia et al., 2024; Muhs et al., 2011), and because the coral CUB19.25 underwent uplift between its formation and MIS 5a, it possibly has formed at a greater depth than that at which the MIS 5a corals formed (depth of life of the species *Dichocoenia stokesii* between 0 and − 20 m, Aronson et al., 2008).

At site 3 (Rancho Cruz), the only age obtained on the lowermost terrace (134.4 ± 0.5 ka, CUB 22.64, Supplementary Table 1) is an open-system age because the measured $\delta^{234}U$ initial value of the fossil coral is slightly higher than that of current sea conditions (~160 ‰ compared with 145 ± 5 ‰, Chutcharavan et al., 2018). An initial excess of ^{234}U produces an overestimation of the ages by U/Th dating (Thompson et al., 2003). If its age is overestimated, the terrace was probably formed during the MIS 5e. I We can therefore infer that the Rancho Cruz terrace formed during this interglacial stage.

At site 4 (Western Siboney), two corals, CUB 19.08 and CUB 19.09, yielded ages of around 130 ka, and one coral (CUB 19.13) yielded an open-system age of around 140 ka (Supplementary Table 1). We propose an MIS 5e age for this terrace. At site 7 (Bate Bate), the two corals dated to 121 ka and 123 ka are associated to the MIS 5e sea level peak (Supplementary Table 1).

5.3. Late quaternary uplift rates

We derive eustasy-corrected uplift rates from the inner edge elevations of dated coastal terraces, once correlated to the nearest highstand (e.g., Pedoja et al., 2018; de Gelder et al., 2020) (Fig. 12). At Cabo Cruz

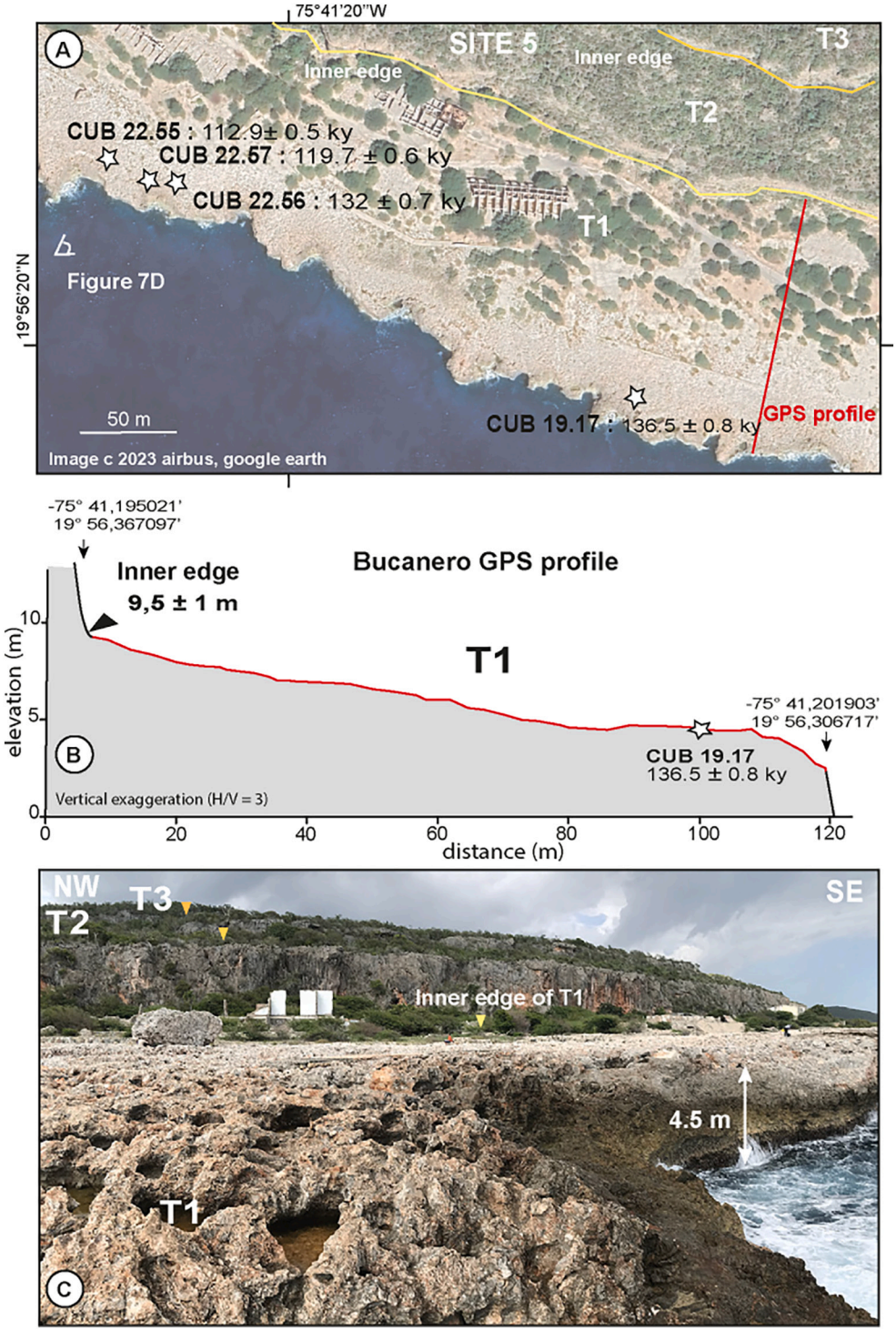

Fig. 7. The coastal sequence at Bucanero (site 5 on Fig. 2). A) General view from satellite imagery with samples and GPS locations, B) dGPS profile and sampling locations. C) Interpreted field picture.

(site 1), the eustasy-corrected uplift rate is -0.02 ± 0.03 mm.yr^{-1} (Table 2). 30 km eastward, at site Boca del Toro (site 2), the uplift rate peaks at 0.17 ± 0.03 mm.yr^{-1} from T1 correlated to MIS 5a highstand (Table 2).

At Rancho Cruz site (site 3), in the central part of the southern coast of Cuba (Fig. 2), the calculated eustasy-corrected uplift rate is 0.02 ± 0.03 mm.yr^{-1}, assuming that T1 is associated with MIS 5e (Table 2). At Western Siboney site (site 4), 25 km westward of site 3, the uplift rate is 0.03 ± 0.03 mm.yr^{-1} from T1 correlated to MIS 5e highstand (Fig. 12). At Bucanero (site 5), the uplift rate is 0.04 ± 0.03 mm yr^{-1}. T1 terrace of Verraco site (site 6) is the same T1 than sites 4 and 5 according to their position on the staked swath profile (site 6, 10 km southeastward of site 5; Fig. 11). But without U/Th ages, we cannot calculate an uplift rate for this site. We have only deduced that it could be higher than for sites 4 and 5 according to the gradual eastward increase of T1 elevation visible on the swath profiles of the area (Fig. 11). Muhs et al. (2017) calculated uplift rates ranging from 0.02 to 0.11 mm.yr^{-1} in Guantanamo Bay (Fig. 12). At Bate Bate site (site 7), in the eastern part of the southern

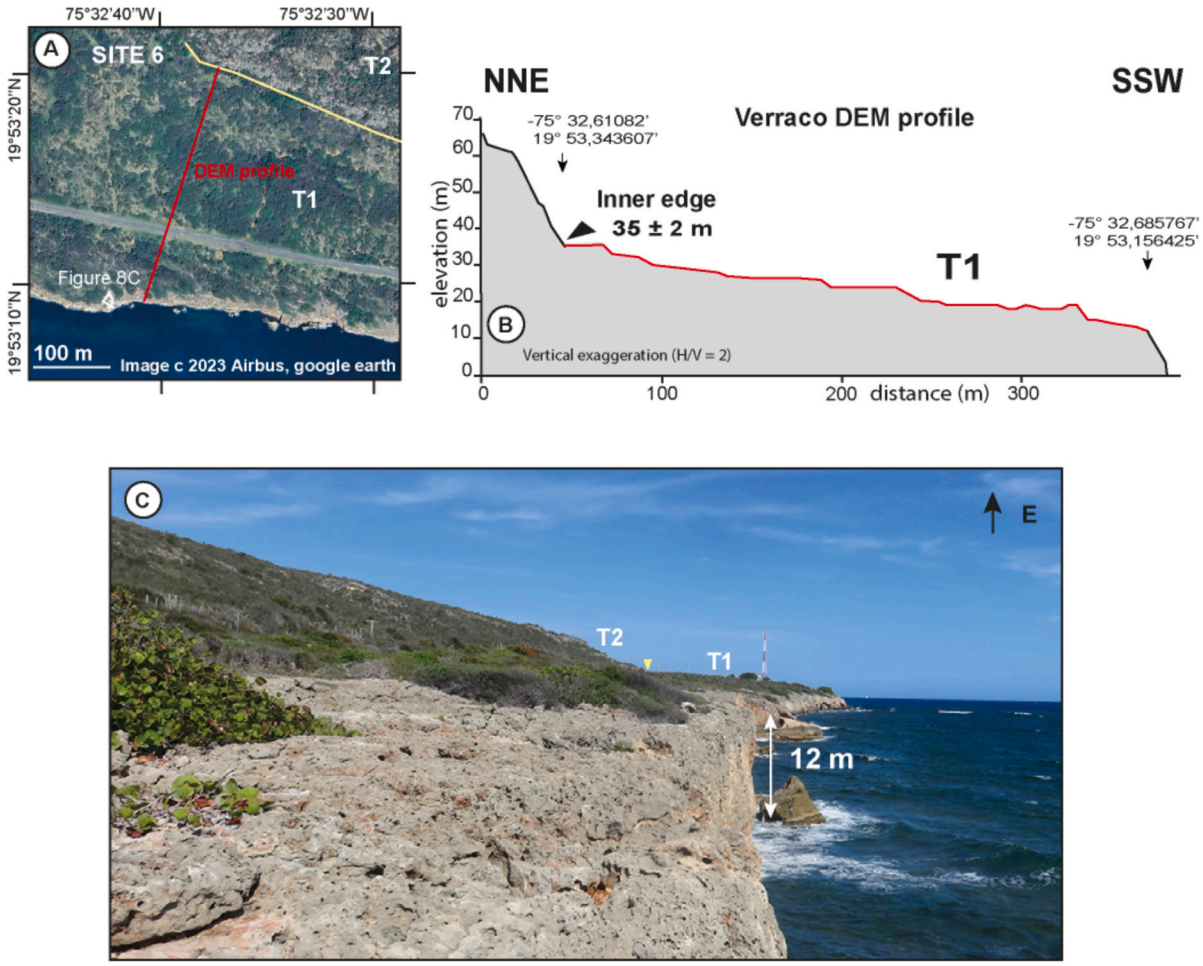

Fig. 8. The coastal sequence at Verraco site (site 6 of Fig. 2). A) General view from satellite imagery with DEM profile location, B) Topographic profile from DEM measurements. C) Field picture of the inner edge of the lowermost coastal terrace.

coast of Cuba, 60 km west of Punta Maísi, the uplift rate is 0.05 ± 0.02 mm.yr $^{-1}$ Authemayou et al. (2023) obtained uplift rates from 0.03 ± 0.04 at Rio Seco site to 0.23 ± 0.07 mm.yr^{-1} at the southern coast of Punta Maísi (Fig. 12).

This set of uplift rates, combined with earlier rates from Muhs et al. (2017) in Guantanamo Bay (blue squares, Fig. 12) and from Authemayou et al. (2023) at Maísi peninsula (green squares, Fig. 12), comprehensively cover the southern coast of Cuba. Maximum Late Quaternary uplift rates are found at three widely separated sites (far east, central, and far west).

5.4. *Onshore/offshore deformation pattern along the Oriente Fault Zone*

In the western part of the coast of southern Cuba, variations in uplift rates are correlated to NW-directed tilting of the coast certainly due to the activity of NE-SW-striking normal faults (White lines in Figs. 12, 13). In particular, secondary faults of this order have been identified as affecting the higher-elevation coastal terraces (Figs. 11H, G). At the Cabo Cruz site, there is no uplift and possibly some subsidence because this site is located on the lower block of a NE-trending secondary normal fault, far from the fault plane. The tilting of the block produces uplift close to the fault plane at the Boca del Toro site, but subsidence far from the fault plane at the Cabo Cruz site. These normal faults are comparable to their offshore counterparts in Cabo Cruz basin. This basin is a pull-apart basin connecting two transform fault segments of the OFZ and associated with active NE-SW striking normal faults (Fig. 12, Calais and de Lepinay, 1991; Perrot et al., 1997). However, the active coastal faults in Cuba are located outside the pull-apart basin. Their occurrence is therefore not only restricted to the pull-apart basin activity and must be related to a larger scale geodynamic process.

The pull-apart basin marks the transition from a fault trace along the toe of the Cayman ridge all the way to the mid-Cayman spreading center, to a segmented trace along the South Cuban margin (Figs. 1, 13). This transition is associated with a change in seismicity and fault-locking depth along the transform fault (OFZ), and in the rheology and thickness of the GonavTen Brink and Lin, 2004; Hayman et al., 2011; Calais et al., 2023; Moreno Toiran et al., 2023) (Fig. 13). There, the Gonave block changes from 5 to 6 km-thick oceanic crust through the west to a ~ 25 km-thick crust through the east (Leroy et al., 2000; Ten Brink and Lin, 2004; Moreno Toiran et al., 2023). In the oceanic crust zone, serpentine enrichment along the fault may favor creeping mechanism (Liu et al., 2020; Calais et al., 2023). The combination of crustal thickness and rheological rock properties variations along the transform fault could thus produce a lateral change of shallow locking/creeping segment with a deep locking segment to the east along the transform fault (Calais et al., 2023). In addition, to the east, the oblique convergence of the Bahamas platform against the Gonave block may increase the coupling between the two plates.

Lower coupling along the western fault segment of the OFZ, compared with the eastern transform fault segment, may explain the intraplate deformation pattern in the North America plate (onshore Cuba). The North America plate moves more easily westward relative to the Gonave block where it is bounded by the creeping fault segment of the OFZ west of Cuba (Calais et al., 2023). This westward increase of

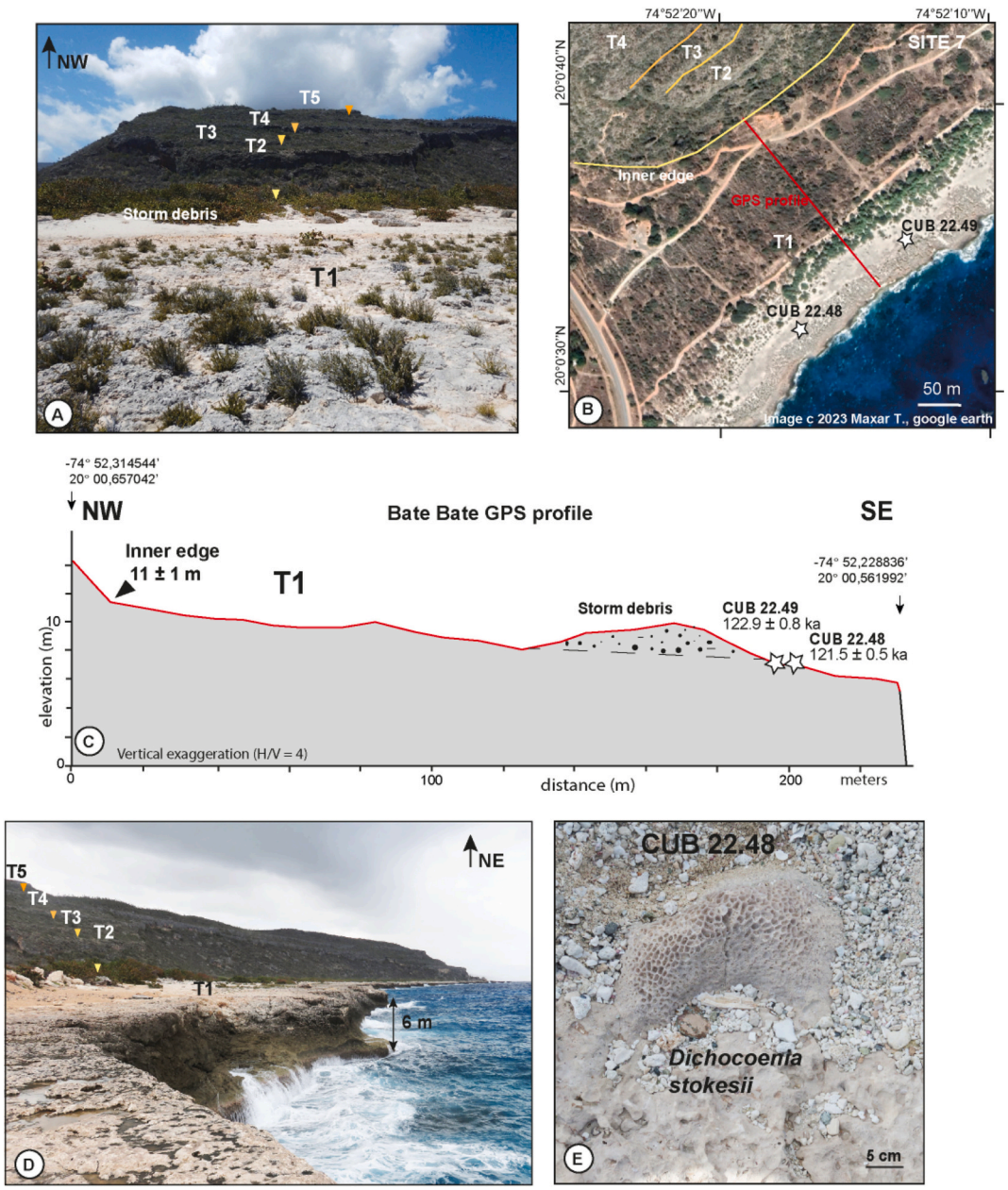

Fig. 9. The coastal sequence at Bate Bate (site 7 of Fig. 2). A) Interpreted picture of the sequence. B) View from satellite imagery with samples and dGPS profile locations, C) dGPS profile. C) and D) Interpreted field picture of the inner edge of T1 and picture of the sampled Dichocoenia stokessi coral colonies.

motion produces NE-SW-striking normal faults that limit the fast west zone from the slower east zone of the North America plate (Fig. 13). South of the creeping transform fault segment of the OFZ (Fig. 13), offshore N-S striking reverse faults are active across the rheological transition zone of the Gonave block between the oceanic crust and the ante-Eocene crust (Montego ridges, Leroy et al., 1996). The reverse faults could be activated by an eastward decrease in the relative movement of the Gonave block slowed by the strong coupling along the eastern locking fault segment of the OFZ (Fig. 13).

The normal faults of the North America plate along the Cabo Cruz coast may also belong to an uncharted pull-apart basin. Indeed, to the north of Cabo Cruz, the ENE-WSE-striking left lateral strike-slip Cauto Nipe fault zone (Cotilla-Rodríguez and Córdoba-Barba, 2010; Vázquez-Taset et al., 2020) could have been the active structure that was the source of the 18 October 1551 earthquake of intensity IX on the MSK intensity scale around the Bayamo earthquake (Fig. 13, Cotilla-Rodríguez and Córdoba-Barba, 2010). Data from GPS networks in the region suggest residual movement to the south of this fault relative to the fixed North American plate north to the fault (Calais et al., 2023). The fault forms a wedge to the west with the OFZ, which could locally promote internal extensional deformation in line with the activity of the NE-SW-striking normal faults along the coast clearly shown in Fig. 12.

In the central zone of the southeastern Cuban coast, uplift is produced by NW-SE-trending folds, north of a transpressive relay zone between two segments of the OFZ between the Gonave ante Eocene crust with low lithospheric depth and the Gonave ante Eocene crust with high lithospheric depth (Figs. 11, 13). To the east of this zone, the OFZ is flanked to the south by the EW-trending Santiago fold-and- thrust belt (SDB) (Calais and Mercier de Lépinay, 1991, Fig. 13). The reverse faults of this belt are very active according to the seismic activity and focal mechanisms recorded in this area (Fig. 13). To the north-east of the SDB, the coastal uplift rate is moderate (Muhs et al., 2017; sites 1 and 2 of Authemayou et al., 2023 and site 7 of this study; Figs. 2, 12). The uplift rates remain greater than 0.02 mm.yr^{-1} (Figs. 12, 13). A component of

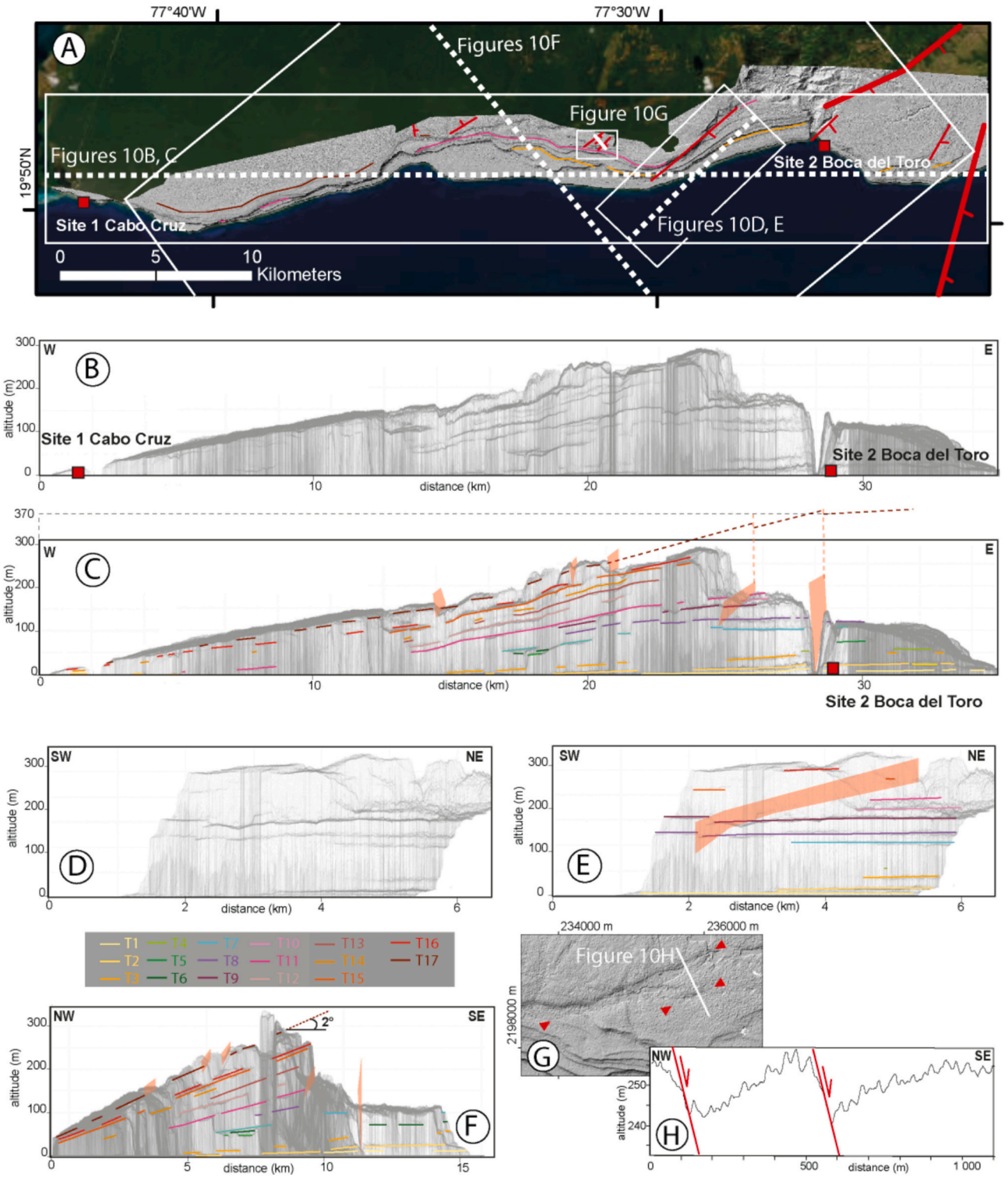

Fig. 10. Deformations of long-lasting coastal terrace sequences in the western part of southern Cuba (see location in Fig. 2). (A) Location map of the stacked swath profiles of coastal terraces with fault trace in red (bold trace corresponding to major faults) on hillshade of high-resolution Pleiades DEM above the satellite imagery, Raw (B) and interpreted (C) W-E-trending stacked swath profiles (trend along the main coast). Raw (D) and interpreted (E) SW-NE-trending stacked swath profiles. Colored lines are inner edge of marine terraces and red parallelograms are fault planes. (F) NW-SE-trending stacked interpreted swath profile. (G) Hillshade of high-resolution Pleiades DEM on secondary normal faults (fault traces shown by red triangles) affecting the upper coastal terraces (coordinate system WGS 84 UTM Zone 18 N). Location in Fig. 10A. (H) Topographic profile across these secondary normal faults. Location in Fig. 10G. (For interpretation of the references to colour in this figure legend, the reader is referred to the web version of this article.)

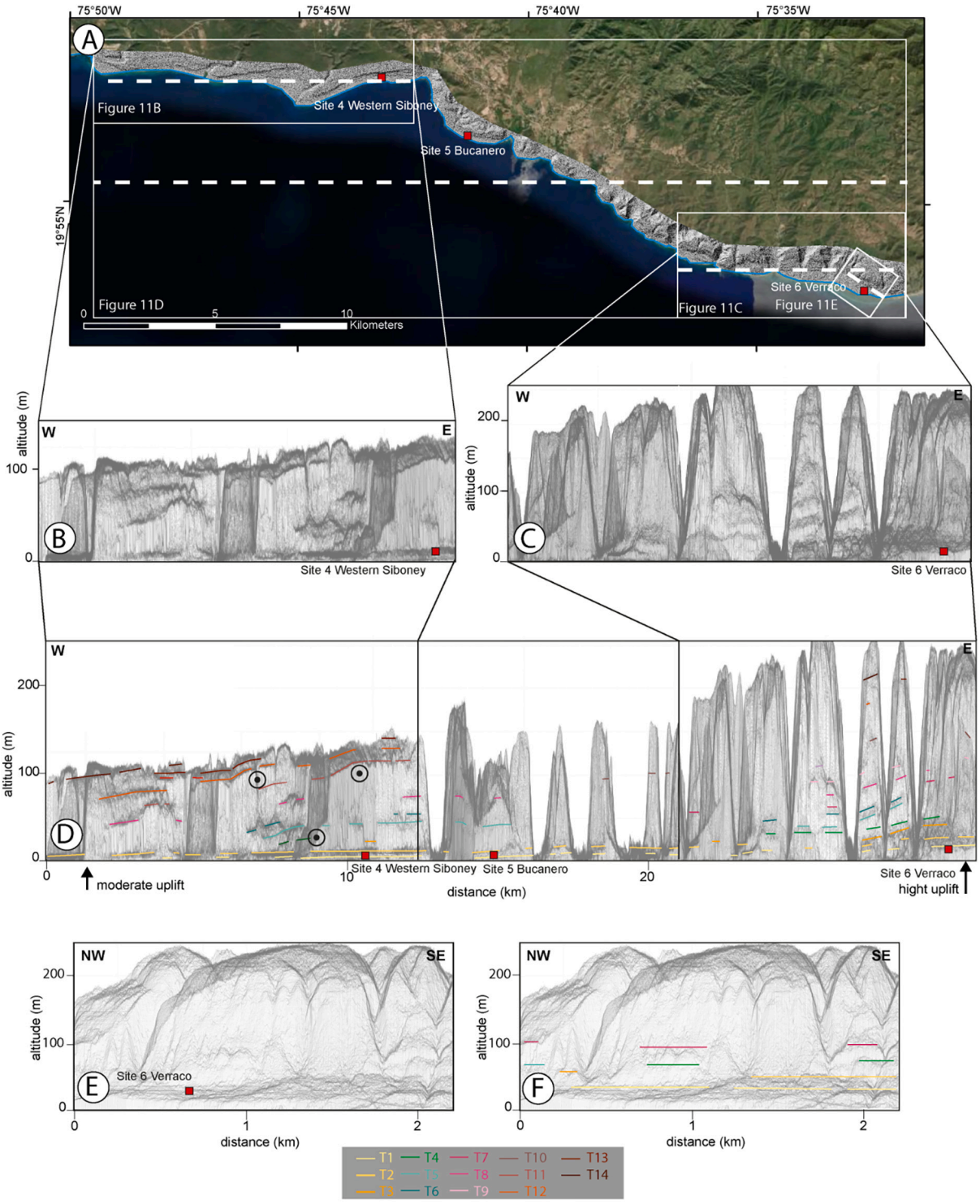

Fig. 11. Deformations of long-lasting coastal terrace sequences in the central part of southern Cuba (see location in Fig. 2). (A) Location map of the stacked swath profiles of coastal terraces on hillshade of high-resolution Pleiades DEM above the satellite imagery, (B) W-E-trending stacked swath profiles to the west. (C) W-E-trending stacked swath profiles to the east. (D) Interpreted W-E-trending stacked swath profiles. (E) NW-SE-trending stacked swath profiles. (F) Interpreted NW-SE-trending stacked swath profiles. Each colored lines is inner edge of coastal terraces, and each circled dot is an anticlinal fold axis.

this uplift is linked to the oblique convergence of the Bahamas platform towards the Gonave block. It is also in this zone that the lithosphere of the Gonave block is thickening rapidly (Moreno Toiran et al., 2023). This variation in thickness could increase the interplate coupling and consequently favor the intraplate shortening in Cuba through coastal folding and in the Gonave plate through the Santiago fold-and-thrust belt, particularly in the zone where the lithosphere is thinning towards the west (Fig. 13). This mechanical change along the OFZ may also explain the more intense seismicity reaching depths up to 80 km along the eastern margin of Cuba (Moreno et al., 2002; Moreno Toiran et al., 2023).

At Punta Maísi, on the southeastern tip of Cuba, high uplift rates are probably linked to submarine E-W-striking thrusts parallel to the OFZ (Authemayou et al., 2023, Figs. 12, 13). In this area, the Bahamas

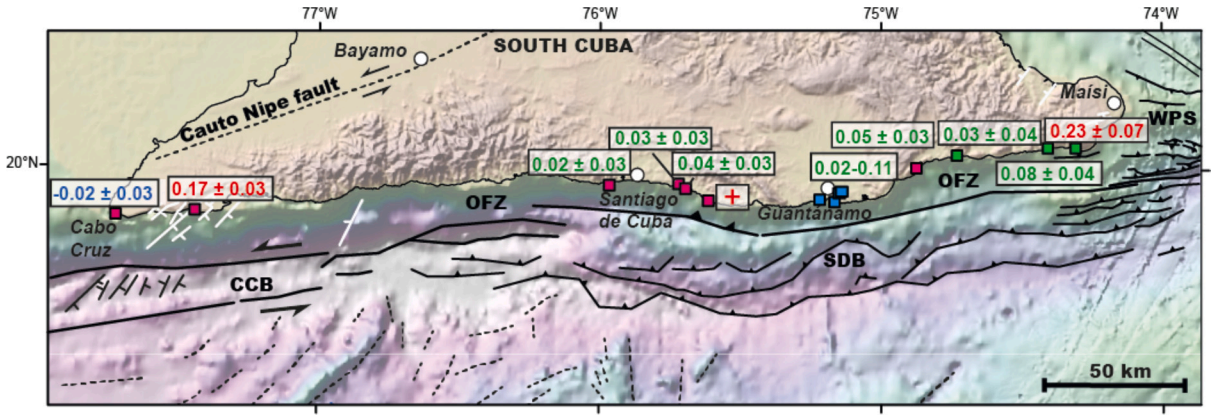

Fig. 12. Onshore uplift rates at sampled sites (values framed by a solid black rectangle) (red squares from our study; blue squares from Muhs et al., 2017; red squares from Authemayou et al., 2023). Onshore active faults are mapped from Magaz García et al. (1997) and Cotilla-Rodriguez and Córdoba-Barba (2010) and offshore structural map, dotted and solid black lines correspond to faults from Calais and Mercier de Lépinay (1991); Leroy et al. (2015) and Oliveira de Sá et al. (2021) and white lines correspond to faults from Authemayou et al. (2023) and this study. Dotted black lines are non-active faults, solid black lines are active faults. CCB: Cabo Cruz Basin, OFZ: Oriente Septentrional Fault Zone; SDB: Santiago Deformed Belt; WPS: Windward Passage Sill. (For interpretation of the references to colour in this figure legend, the reader is referred to the web version of this article.)

Table 2
Uplift rates calculated as a function of age and elevation of the inner edge of each low-standing coastal terrace in this study. Lines in bold are associated with the preferred terrace age hypothesis.

Site	Coastal terrace	MIS Age	Inner edge elevation	Estimated paleo-sea level	uplift rate
		(kyr)	(m)	(m)	(mm yr^{-1})
1	T1 Cabo Cruz	115–130	2,6 ± 1	2–8 (Muhs et al., 2011)	−0,019 ± 0,031
2	T1 Boca de Toro	76–88	8 ± 1	−6,5 to −5,1 (Hsia et al., 2024)	0,171 ± 0,033
3	T1 Rancho Cruz	115–130	7 ± 1	2–8 (Muhs et al., 2011)	0,017 ± 0,035
4	T1 Western Siboney	115–130	8 ± 1	2–8 (Muhs et al., 2011)	0,026 ± 0,035
5	T1 Bucanero	115–130	9,5 ± 1	2–8 (Muhs et al., 2011)	0,039 ± 0,035
7	T1 Bate Bate	115–130	11 ± 1	2–8 (Muhs et al., 2011)	0,051 ± 0,036

platform cannot easily underthrust behind the North Cuba Fault Zone (NCFZ) (the western extension of the North Hispaniola Fault Zone, NHFZ in Fig. 13) due to its continental crust rheology and thickness (Fig. 13; Oliveira de Sá et al., 2021; Oliviera de Sá et al., 2024; Oliveira de Sá, 2023). Shortening is thus concentrated in the upper plate in the Windward Passage Sill (WPS) and the southeastern zone of Cuba by E-W-striking thrusting and folding producing high coastal uplift in Maísi area (Oliveira de Sá et al., 2021; Oliveira de Sá, 2023; Authemayou et al., 2023, Figs. 12, 13).

6. Conclusion

We studied seven sites along the southeastern coast of Cuba. We performed topographic swath profiles of the sequences of coastal terraces, high resolution topographic profiles and U/Th dating on 18 coral samples, which enable us to correlate the lowermost coastal terraces with MIS 5. These data revealed lateral variations in coastal uplift along the OFZ transform fault with late Quaternary uplift rates ranging from -0.02 ± 0.02 to 0.23 ± 0.07 mm.yr^{-1}. Two fast uplifting zones have been detected at the eastern and western ends of the southern coast. They can be respectively assigned to NE-SW normal faulting north of a pull-apart basin between two segments of the OFZ and E-W-striking reverse faulting offshore parallel to the OFZ. The first western zone is correlated with changes in the nature and crustal to lithospheric depth of the Gonave block to the south of the transform fault, linked to the lateral transition from an oceanic crust to a passive margin crust with an arc affinity. The easternmost zone is associated with the oblique collision of the continental Bahamas platform which can no longer underthrust behind the North Hispaniola/North Cuba fault zone.

Data avaibility

The topographic data (longitude, latitude coverage of −74,40°; 20,30° and − 77,45°; 19.55°) used in this study is available at: http://www.latitude-geosystems.com [Dataset], Pleiades' satellite imagery was obtained through the ISIS program of the CNES under an academic license and is not for open distribution. On request, we will provide the DSM calculated from this imagery to any academic researcher who gets approval from CNES (contact isis-pleiades@cnes.fr quoting this paper, Christine.authemayou@univ-brest.fr in copy).The ESRI's ArcGIS 10 software is available at:https://www.esri.com [Software], U/Th data are integrated into the manuscript in Supplementary Table 1. Uplift rates were calculated from this data and elevation values are indicated in Table 2.

CRediT authorship contribution statement

Christine Authemayou: Writing – original draft, Supervision, Project administration, Methodology, Investigation, Funding acquisition, Formal analysis, Data curation, Conceptualization. **Leandro Penalver:** Writing – review & editing, Project administration, Investigation, Funding acquisition, Conceptualization. **Denovan Chauveau:** Writing – review & editing, Investigation, Conceptualization. **Kevin Pedoja:** Writing – review & editing, Methodology, Investigation, Conceptualization. **Pedro Dunan Avila:** Writing – review & editing, Investigation. **Arelis Nunez:** Writing – review & editing, Project administration, Investigation. **Pedro Benítez Frometa:** Writing – review & editing, Investigation. **Edwige Pons Branchu:** Writing – review & editing, Investigation, Data curation. **Alexino Progam:** Investigation. **Denyse Martin Izquierdo:** Investigation. **Gino de Gelder:** Writing – review & editing, Investigation. **Julie Perrot:** Writing – review & editing, Formal analysis. **Ramon Rivada:** Investigation. **Enrique Diego Arango-Arias:** Investigation. **Laurent Husson:** Writing – review & editing.

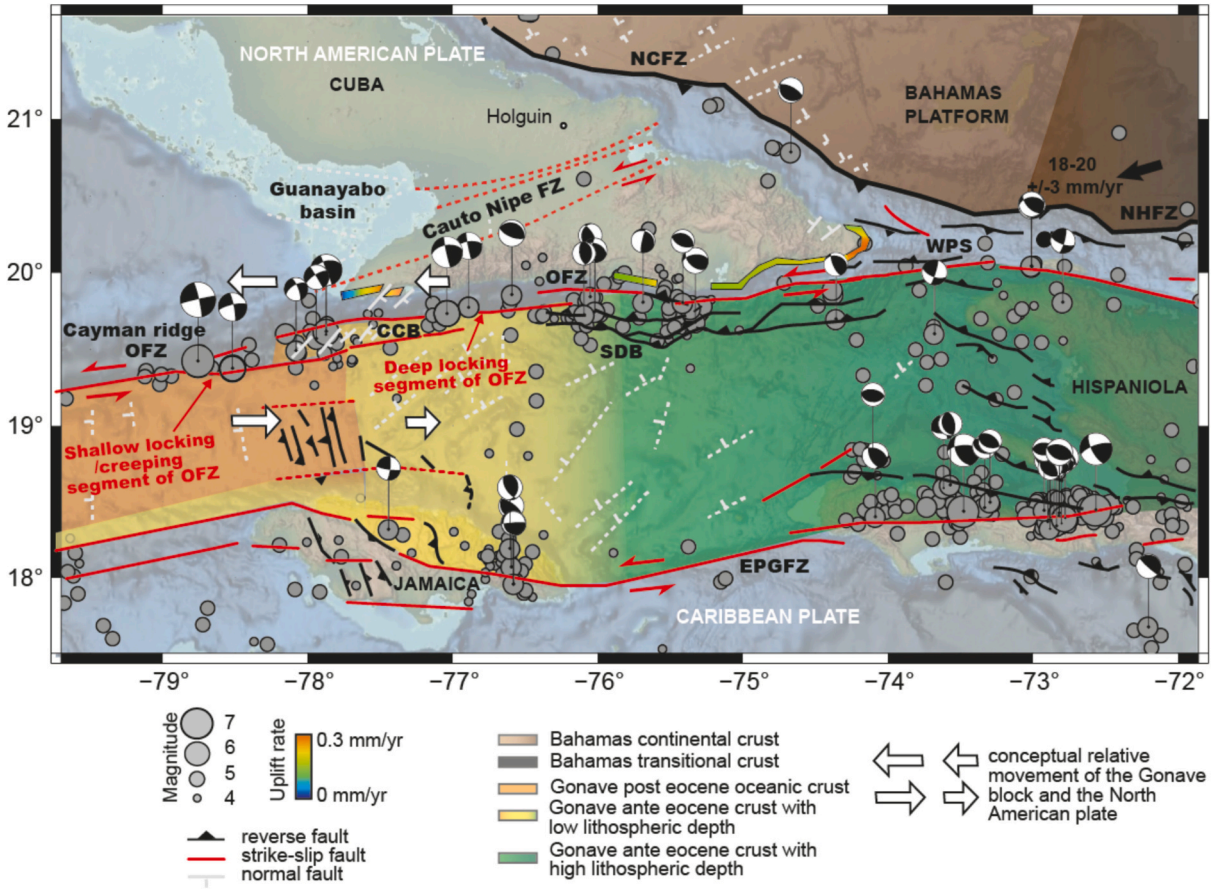

Fig. 13. Structural map, crustal nature, and uplift rate lateral variations along the northern Caribbean boundary from Calais and Mercier de Lepinay (1991); Leroy et al. (1996), (2015); Hayman et al. (2011); Oliveira de Sá et al. (2021); Authemayou et al. (2023); Moreno Toiran et al. (2023); Oliveira de Sá (2023); Calais et al. (2023) and this study. Dashed lines correspond to supposed or inactive faults. The M > 3 seismicity from 1978 to october 2024 from the USGS/NEIC catalog and the focal mechanisms for Mw > 5 earthquakes from the gCMT database. Green line is the isoseismal of I = 8 and 9 of the Bayamo earthquake in 1551 according to Cotilla-Rodríguez and Córdoba-Barba, 2010. NHFZ: North Hispaniola Fault Zone, NCFZ: North Cuba Fault Zone, CCB: Cabo Cruz Basin, OFZ: Oriente Fault Zone; EPGFZ: Enriquillo-Plantain-Garden Fault Zone; WPS: Windward Passage Sill; SDB: Santiago Deformed Belt.

Declaration of competing interest

The authors declare that they have no known competing financial interests or personal relationships that could have appeared to influence the work reported in this paper.

Acknowledgements

This work was supported by public funds received in the framework of a project (ANR-10-EQPX-20) of the program "Investissements d'Avenir" managed by the French National Research Agency. It was also supported by ISblue projects, Interdisciplinary graduate school for the blue planet (ANR-17-EURE-0015, BIOTEDYCO), A National INSU TelluS project (TECIBO), the PHC Carlos Scientific Cooperation Program (N49740YL) and co-funded by a grant from the French government under the program "Investissements d'Avenir" embedded in France 2030 (VuCoRem project, C. Authemayou) and the CNES TOSCA program (CETTROPICO, C. Authemayou). Constructive reviews by Daniel R. Muhs and two other reviewers greatly helped to improve this manuscript.

Appendix A. Supplementary data

Supplementary data to this article can be found online at https://doi.org/10.1016/j.tecto.2025.230789.

Data availability

Data will be made available on request.

References

Agassiz, A., 1894. A Reconnaissance of the Bahamas and of the Elevated Reefs of Cuba in the Steam Yacht" Wild Duck", January to April, 1893 (Vol. 26, no. 1). Museum.

Armijo, R., Lacassin, R., Coudurier-Curveur, A., & Carrizo, D. (2015). Coupled tectonic evolution of Andean orogeny and global climate. Earth Sci. Rev., 143, 1–35. doi: 10..1016/j.earscirev.2015.01.005.

Aronson, R., Bruckner, A., Moore, J., Precht, B., Weil, E., 2008. [Various Coral Species Treatments] in: IUCN 2010. IUCN Red List of Threatened Species. Version 2010.4. www.iucnredlist.org.

Authemayou, C., Nuñez, A., Pedoja, K., Peñalver, L., Chauveau, D., Dunán-Avila, P., Anne-Morwenn, P., 2023. Oblique collision of the Bahamas platform at the northern boundary of the Caribbean plate recorded by the late cenozoic coastal terraces of SE Cuba. Tectonics 42 (8).

Barlow, N.L., McClymont, E.L., Whitehouse, P.L., Stokes, C.R., Jamieson, S.S., Woodroffe, S.A., Sanchez-Montes, M.L., 2018. Lack of evidence for a substantial sea-level fluctuation within the Last Interglacial. Nature Geosci. 11 (9), 627–634.

Bar-Matthews, M., Wasserburg, G.J., Chen, J.H., 1993. Diagenesis of fossil coral skeletons: correlation between trace elements, textures, and 234U238U. Geochim. Cosmochim. Acta 57 (2), 257–276. https://doi.org/10.1016/0016–7037(93)90429-Z.

Boschman, L.M., van Hinsbergen, D.J., Torsvik, T.H., Spakman, W., Pindell, J.L., 2014. Kinematic reconstruction of the Caribbean region since the early Jurassic. Earth Sci. Rev. 138, 102–136. https://doi.org/10.1029/2023TC007806.

Burke, K., 1988. Tectonic evolution of the Caribbean. Annu. Rev. Earth Planet. Sci. 16 (1), 201–230. https://doi.org/10.1146/annurev.ea.16.050188.001221.

Calais, E., de Lepinay, B.M., 1991. From transtension to transpression along the northern Caribbean plate boundary off Cuba: Implications for the recent motion of the Caribbean plate. Tectonophysics 186 (3–4), 329–350.

Calais, E., De Lépinay, B.M., 1995. Strike-slip tectonic processes in the northern Caribbean between Cuba and Hispaniola (Windward Passage). Mar. Geophys. Res. 17, 63–95. https://doi.org/10.1007/BF01268051.
Calais, E., Mercier de Lépinay, B., 1991. From transtension to transpression along the northern Caribbean transcurrent plate boundary off Cuba: implications for the recent motion of the Caribbean plate. Tectonophysics 186, 329–350. https://doi.org/10.1016/0040–1951(91)90367–2.
Calais, E., Béthoux, N., de Lépinay, B.M., 1992. From transcurrent faulting to frontal subduction: a seismotectonic study of the northern Caribbean plate boundary from Cuba to Puerto Rico. Tectonics 11 (1), 114–123. https://doi.org/10.1029/91TC02364.
Calais, E., Symithe, S., de Lepinay, B.M., Prépetit, C., 2016. Plate boundary segmentation in the northeastern Caribbean from geodetic measurements and Neogene geological observations. Compt. Rendus Geosci. 348 (1), 42–51. https://doi.org/10.1016/j.crte.2015.10.007.
Calais, E., Gonzalez, O.F., Arango-Arias, E.D., Moreno, B., Palau, R., Cutie, M., Symithe, S., 2023. Current deformation along the northern Caribbean plate boundary from GNSS measurements in Cuba. Tectonophysics 868, 230068. https://doi.org/10.1016/j.tecto.2023.230068.
Chauveau, D., Authemayou, C., Pedoja, K., Molliex, S., Husson, L., Scholz, D., Aster Team, 2021. On the generation and degradation of emerged coral reef terrace sequences: first cosmogenic 36Cl analysis at Cape Laundi, Sumba Island (Indonesia). Quat. Sci. Rev. 269, 107144. https://doi.org/10.1016/j.quascirev.2021.107144.
Chauveau, D., Pastier, A.M., de Gelder, G., Husson, L., Authemayou, C., Pedoja, K., Cahyarini, S.Y., 2024a. Unravelling the morphogenesis of coastal terraces at Cape Laundi (Sumba Island, Indonesia): insights from numerical models. Earth Surf. Process. Landf. 49 (2), 549–566. https://doi.org/10.1002/esp.5720.
Chauveau, D., Georgiou, N., Cerrone, C., Dean, S., Rovere, A., 2024b. Sea-Level Oscillations Within the Last Interglacial: Insights From Coral Reef Stratigraphic Forward Modelling. https://doi.org/10.31223/X59T1V.
Cheng, H., Adkins, J., Edwards, R.L., Boyle, E.A., 2000. U-Th dating of deep-sea corals. Geochim. Cosmochim. Acta 64 (14), 2401–2416.
Cheng, H., Edwards, R. L., Shen, C. C., Polyak, V. J., Asmerom, Y., Woodhead, J., ... & Alexander Jr, E. C. (2013). Improvements in 230Th dating, 230Th and 234U half-life values, and U–Th isotopic measurements by multi-collector inductively coupled plasma mass spectrometry. Earth Planet. Sci. Lett., 371, 82–91. doi: 10.1016/j.epsl.2013.04.006.
Chutcharavan, P.M., Dutton, A., Ellwood, M.J., 2018. Seawater 234U/238U recorded by modern and fossil corals. Geochim. Cosmochim. Acta 224, 1–17.
Corbeau, J., Rolandone, F., Leroy, S., Meyer, B., Mercier de Lépinay, B., Ellouz-Zimmermann, N., Momplaisir, R., 2016. How transpressive is the northern Caribbean plate boundary? Tectonics 35 (4), 1032–1046.
Cotilla-Rodríguez, M.O., Córdoba-Barba, D., 2010. The Bayamo earthquake (Cuba) of the 18 October 1551. Int. J. Geosci. 1 (01), 1. https://doi.org/10.4236/ijg.2010.11001.
Creveling, J.R., Mitrovica, J.X., Clark, P.U., Waelbroeck, C., Pico, T., 2017. Predicted bounds on peak global mean sea level during marine isotope stages 5a and 5c. Quat. Sci. Rev. 163, 193–208.
Crosby, W.O., 1883. Elevated coral reefs of Cuba. Ann. Mag. Nat. Hist. 12 (70), 283–284.
Cruz-Orosa, I., Sàbat, F., Ramos, E., Vázquez-Taset, Y.M., 2012. Synorogenic basins of Central Cuba and collision between the Caribbean and north American plates. Int. Geol. Rev. 54 (8), 876–906. https://doi.org/10.1080/14786448308627438.
Davis, W.M., 1933. Glacial Epochs of the Santa Monica Mountains, California. Bull. Geol. Soc. Am. 44 (5), 1041–1133.
de Gelder, G., Jara-Munoz, J., Melnick, D., Fernández-Blanco, D., Rouby, H., Pedoja, K., Lacassin, R., 2020. How do sea-level curves influence modeled marine terrace sequences? Quat. Sci. Rev. 229, 106132. https://doi.org/10.1016/j.quascirev.2019.106132.
de Gelder, G., Husson, L., Pastier, A.M., Fernández-Blanco, D., Pico, T., Chauveau, D., Pedoja, K., 2022. High interstadial sea levels over the past 420ka from the Huon Peninsula, Papua New Guinea. Commun. Earth Environ. 3 (1), 256. https://doi.org/10.1038/s43247–022–00583-7.
de Gelder, G., Solihuddin, T., Utami, D.A., Hendrizan, M., Rachmayani, R., Chauveau, D., Cahyarini, S.Y., 2023. Geodynamic control on Pleistocene coral reef development: insights from northwest Sumba Island (Indonesia). Earth Surf. Process. Landf. 48 (13), 2536–2553. https://doi.org/10.1002/esp.5643.
del Busto, R., 1975. Las terrazas marinas de Maisí. In: Ciencias Serie 7 Geografía. Centro de Información Científica y Técnica. Universidad de La Habana.
del Corral, J.I., 1944. Terrazas Pleistocénicas Cubanas. Imp. Compañía Editora de Libros y Folletos.
DeMets, C., Jansma, P.E., Mattioli, G.S., Dixon, T.H., Farina, F., Bilham, R., Mann, P., 2000. GPS geodetic constraints on Caribbean-North America plate motion. Geophys. Res. Lett. 27 (3), 437–440. https://doi.org/10.1029/1999GL005436.
Donnelly, M., 1989. International trade in hawksbill sea turtle shell in the wider Caribbean. In: Eckert, S.A., Eckert, K.L., Richardson, T.H. (Eds.), Comps. Proc. 9th Annual Workshop on Sea Turtle Conservation and Biology. NOAA Tech, pp. 45–47. Memo. NMFS-SEFC-232.
Fouke, K.W., Kerans, C., 2024. Evidence for a sea level fall during the last interglacial highstand on West Caicos, Turks and Caicos Islands. Paleoceanogr. Paleoclimatol. 39 (8), e2024PA004879.
Gordon, M.B., Mann, P., Cáceres, D., Flores, R., 1997. Cenozoic tectonic history of the North America-Caribbean plate boundary zone in western Cuba. J. Geophys. Res. Solid Earth 102 (B5), 10055–10082. https://doi.org/10.1029/96JB03177.
Hamelin, B., Bard, E., Zindler, A., Fairbanks, R.G., 1991. 234U/238U mass spectrometry of corals: How accurate is the UTh age of the last interglacial period? Earth Planet. Sci. Lett 106 (1–4), 169–180.
Hastie, A.R., Mitchell, S.F., Treloar, P.J., Kerr, A.C., Neill, I., Barfod, D.N., 2013. Geochemical components in a cretaceous island arc: the Th/La–(Ce/Ce*) Nd diagram and implications for subduction initiation in the inter-American region. Lithos 162, 57–69. https://doi.org/10.1016/j.lithos.2012.12.001.
Hayman, N.W., Grindlay, N.R., Perfit, M.R., Mann, P., Leroy, S., de Lépinay, B.M., 2011. Oceanic core complex development at the ultraslow spreading Mid-Cayman Spreading Center. Geochem. Geophys. Geosyst. 12 (3). https://doi.org/10.1029/2010GC003240.
Hill, R.T., 1895. Notes on the Geology of the Island of Cuba: Based Upon a Reconnoissance Made for Alexander Agassiz, Museum.
Horsfield, W.T., 1975. Quaternary vertical movements in the greater Antilles. Geol. Soc. Am. Bull. 86, 933–938. https://doi.org/10.1130/0016–7606(1975)86<933:QVMITG>2.0.CO;2.
Hsia, S., Toth, L.T., Mortlock, R., Kerans, C., 2024. Re-evaluating Marine Isotope Stage 5a paleo-sea-level trends from across the Florida Keys reef tract. Quatern. Sci. Adv. 15, 100222.
Husson, L., Pastier, A.M., Pedoja, K., Elliot, M., Paillard, D., Authemayou, C., Cahyarini, S.Y., 2018. Reef carbonate productivity during quaternary sea level oscillations. Geochem. Geophys. Geosyst. 19 (4), 1148–1164. https://doi.org/10.1002/2017GC007335.
Iturralde-Vinent, M.A., 1994. Cuban geology: a new plate-tectonic synthesis. J. Pet. Geol. 17 (1), 39–69. https://doi.org/10.1111/j.1747–5457.1994.tb00113.x.
Iturralde-Vinent, M.A., 2003. Ensayo sobre la paleogeografía del Cuaternario de Cuba. In: Memorias V Congreso Cubano de Geología y Minería. CD ROM, La Habana, p. 74. ISBN 959-7117-II-8,.
Iturralde-Vinent, M.A. (Ed.), 2009. Geología de Cuba para todos. Editorial Científico-Técnica.
Iturralde-Vinent, M.A., MacPhee, R.D., 1999. Paleogeography of the Caribbean region: implications for Cenozoic biogeography. Bull. AMNH 238.
Jaffey, A.H., Flynn, K.F., Glendenin, L.E., Bentley, W.T., Essling, A.M., 1971. Precision measurement of half-lives and specific activities of U 235 and U 238. Phys. Rev. C 4 (5), 1889. https://doi.org/10.1103/PhysRevC.4.1889.
Lajoie, K.R., 1986. Coastal tectonics. Active Tecton. 95–124.
Leroy, S., de Lépinay, B.M., Mauffret, A., Pubellier, M., 1996. Structural and tectonic evolution of the eastern Cayman Trough (Caribbean Sea) from seismic reflection data. AAPG Bull. 80 (2), 222–247. https://doi.org/10.1306/64ED8796–1724-11D7-8645000102C1865D.
Leroy, S., Ellouz-Zimmermann, N., Corbeau, J., Rolandone, F., de Lepinay, Meyer, B., Muñoz, S., 2015. Segmentation and kinematics of the North America-Caribbean plate boundary offshore Hispaniola. Terra Nova 27 (6), 467–478.
Leroy, S., Mauffret, A., Patriat, P., Mercier de Lépinay, B., 2000. An alternative interpretation of the Cayman trough evolution from a reidentification of magnetic anomalies. Geophys. J. Int. 141 (3), 539–557. https://doi.org/10.1046/j.1365-246x.2000.00059.x.
Liu, Y., McGuire, J.J., Behn, M.D., 2020. Aseismic transient slip on the Gofar transform fault, east East Pacific Rise. Proc. Natl. Acad. Sci. 117, 10188–10194. https://doi.org/10.1073/pnas.1913625117.
Magaz García, A.R., Díaz Díaz, J.L., Hernández Santana, J.R., 1997. Elementos geomorfológicos básicos para el análisis y determinación de zonas de fallamiento activo en las condiciones de Cuba. Invest. Geog. 9–83.
Mann, P., 1997. Model for the formation of large, transtensional basins in zones of tectonic escape. Geology 25 (3), 211–214. https://doi.org/10.1130/0091–7613(1997)025<0211:MFTFOL>2.3.CO;2.
Mann, P., Schubert, C., Burke, K., 1991. Review of Caribbean Neotectonics. https://doi.org/10.1130/DNAG-GNA-H.307.
Mann, P., Taylor, F.W., Edwards, R.L., Ku, T.L., 1995. Actively evolving microplate formation by oblique collision and sideways motion along strike-slip faults: an example from the northeastern Caribbean plate margin. Tectonophysics 246 (1–3), 1–69. https://doi.org/10.1016/0040–1951(94)00268-E.
Mann, P., Calais, E., Ruegg, J.C., DeMets, C., Jansma, P.E., Mattioli, G.S., 2002. Oblique collision in the northeastern Caribbean from GPS measurements and geological observations. Tectonics 21 (6), 1–7. https://doi.org/10.1029/2001TC001304.
Meinzer, O.E., 1933. Geological reconnaissance adjacent to Guantanamo bay, Cuba. J. Wash. Acad. Sci. 23, 246e260.
Moreno Toiran, B., Aoudia, A., Manu-Marfo, D., Kherchouche, R., Pachhai, S., 2023. Crust–uppermost mantle structure beneath the caribbean region from seismic ambient noise tomography. Bull. Seismol. Soc. 113 (3), 1064–1076.
Moreno, B., Grandison, M., Atakan, K., 2002. Crustal velocity model along the southern Cuban margin: implicationsfor the tectonic regime at an active plate boundary. Geophys. J. Int. 151, 632–645. https://doi.org/10.1046/j.1365-246X.2002.01810.x.
Muhs, D.R., Budahn, J.R., 2009. Geochemical evidence for African dust and volcanic ash inputs to terra rossa soils on carbonate reef terraces, northern Jamaica, West Indies. Quat. Int. 196 (1–2), 13–35.
Muhs, D.R., Schweig, E.S., Simmons, K.R., Halley, R.B., 2017. Late quaternary uplift along the North America-Caribbean plate boundary: evidence from the sea level record of Guantanamo Bay, Cuba. Quat. Sci. Rev. 178, 54–76.
Muhs, D.R., Simmons, K.R., Schumann, R.R., Halley, R.B., 2011. Sea-level history of the past two interglacial periods: new evidence from U-series dating of reef corals from south Florida. Quat. Sci. Rev. 30 (5–6), 570–590.
Murray-Wallace, C.V., Woodroffe, C.D., 2014. Quaternary Sea-Level Changes: A Global Perspective. Cambridge University Press.
Núñez Jiménez, A., 1973. Geografía de Cuba. No Title.
Oliveira de Sá, A., 2023. Relationships between Tectonic and Sedimentary Systems at the Northern Boundary of the Caribbean Plate (Cuba-Hispaniola). Geodynamic Implications. Doctoral thesis.

Oliveira de Sá, A., d'Acremont, E., Leroy, S., Lafuerza, S., 2021. Polyphase deformation and strain migration on the septentrional-oriente fault zone in the windward passage, Northern Caribbean Plate Boundary. Tectonics 40 (8), e2021TC006802. https://doi.org/10.1029/2021TC006802.

Oliviera de Sá, A., Leroy, S., d'Acremont, E., Lafuerza, S., Granja-Bruña, J.L., Moreno, B., Letouzey, J., 2024. The protracted evolution of a plate boundary: Eastern Cuba block and Old Bahamas Channel. Geochem. Geophys. Geosyst. 25 (5), e2023GC011230.

Pastier, A.M., Husson, L., Pedoja, K., Bézos, A., Authemayou, C., Arias-Ruiz, C., Cahyarini, S.Y., 2019. Genesis and architecture of sequences of Quaternary coral reef terraces: insights from numerical models. Geochem. Geophys. Geosyst. 20 (8), 4248–4272. https://doi.org/10.1029/2019GC008239.

Pedoja, K., Husson, L., Regard, V., Cobbold, P.R., Ostanciaux, E., Johnson, M.E., Delcaillau, B., 2011. Relative Sea-level fall since the last interglacial stage: are coasts uplifting worldwide? Earth Sci. Rev. 108 (1–2), 1–15. https://doi.org/10.1016/j.earscirev.2011.05.002.

Pedoja, K., Husson, L., Johnson, M.E., Melnick, D., Witt, C., Pochat, S., Garestier, F., 2014. Coastal staircase sequences reflecting sea-level oscillations and tectonic uplift during the Quaternary and Neogene. Earth Sci. Rev. 132, 13–38. https://doi.org/10.1016/j.earscirev.2014.01.007.

Pedoja, K., Dunán-Avila, P., Jara-Muñoz, J., Authemayou, C., Nuñez-Labañino, A., De Gelder, G., Regard, V., 2023. On a~ 210 t Caribbean coastal boulder: The huracanolito seaward of the ruins of the Bucanero resort, Juragua, Oriente, Cuba. Earth Surf. Process. Landf. 48 (15), 3074–3090.

Pedoja, K., Husson, L., Bézos, A., Pastier, A.M., Imran, A.M., Arias-Ruiz, C., Choblet, G., 2018. On the long-lasting sequences of coral reef terraces from SE Sulawesi (Indonesia): distribution, formation, and global significance. Quat. Sci. Rev. 188, 37–57. https://doi.org/10.1016/j.quascirev.2018.03.033.

Peñalver, L.L., Castellanos, E., Perez, R., Rivada, R., 2003. Las terrazas marinas de Cuba y su correlacon con algunas del area circumcaribe. In: Geologia del Cuaternario, Geomorfologa̋a y Carso. La Habana, Memorias Geominerales, pp. 1–10.

Peñalver, L., Pedoja, K., Martin-Izquierdo, D., Authemayou, C., Nuñez, A., Chauveau, D., Husson, L., 2021. The Cuban staircase sequences of coral reef and marine terraces: a forgotten masterpiece of the Caribbean geodynamical puzzle. Mar. Geol. 440, 106575. https://doi.org/10.1016/j.margeo.2021.106575.

Perrot, J., Calais, E., Mercier de Lépinay, B., 1997. Tectonic and kinematic regime along the Northern Caribbean Plate Boundary: new insights from broad-band modeling of the May 25, 1992, Ms= 6.9 Cabo Cruz, Cuba, earthquake. Pure Appl. Geophys. 149, 475–487. https://doi.org/10.1007/s000240050036.

Pindell, J., Dewey, J.F., 1982. Permo-Triassic reconstruction of western Pangea and the evolution of the Gulf of Mexico/Caribbean region. Tectonics 1 (2), 179–211. https://doi.org/10.1029/TC001i002p00179.

Pindell, J., Kennan, L., Maresch, W.V., Stanek, K., Draper, G., Higgs, R., 2005. Plate-kinematics and crustal dynamics of circum-Caribbean arc-continent interactions: tectonic controls on basin development in Proto-Caribbean margins. Spec. Pap. Geol. Soc. Am. 394, 7.

Pindell, J., Maresch, W.V., Martens, U., Stanek, K., 2012. The Greater Antillean Arc: early cretaceous origin and proposed relationship to central American subduction mélanges: implications for models of Caribbean evolution. Int. Geol. Rev. 54 (2), 131–143. https://doi.org/10.1080/00206814.2010.510008.

Pons-Branchu, E., Hillaire-Marcel, C., Ghaleb, B., Deschamps, P., Sinclair, D., 2005. Early diagenesis impact on precise U-series dating of deep-sea corals. Example of a 100-200 years old *Lophelia Pertusa* sample from NE Atlantic. Geochim. Cosmochim. Acta 69 (20), 4865–4879. https://doi.org/10.1016/j.gca.2005.06.011.

Pons-Branchu, E., Barbarand, J., Caffy, I., Dapoigny, A., Drugat, L., Dumoulin, J.P., Valladas, H., 2022. U-series and radiocarbon cross dating of speleothems from Nerja Cave (Spain): evidence of open system behavior. Implication for the Spanish rock art chronology. Quat. Sci. Rev. 290, 107634.

Pubellier, M., Mauffret, A., Leroy, S., Vila, M., Amilcar, H., 2000. Plate boundary readjustment in oblique convergence: example of the Neogene of Hispaniola, Greater Antilles. Tectonics 19 (4), 630–648. https://doi.org/10.1029/2000TC900007.

Ramos, J.P., Mann, P., 2023. Late cretaceous-recent tectonostratigraphic evolution of the Yucatan back-Arc basin, northern Caribbean Sea. Geochem. Geophys. Geosyst. 24 (8), e2023GC010933. https://doi.org/10.1029/2023GC010933.

Ribot, M., Lefèvre, M., Klinger, Y., Pons-Branchu, E., Dapoigny, A., Jónsson, S., 2024. Vertical deformation along a strike-slip plate boundary: the uplifted marine terraces of the Gulf of Aqaba and Tiran Island, at the southern end of the Dead Sea Fault. Tectonics 43 (9), e2023TC007977.

Rojas-Agramonte, Y., Neubauer, F., Handler, R., García-Delgado, D.E., Friedl, G., Delgado-Damas, R., 2005. Variation of palaeostress patterns along the Oriente transform wrench corridor, Cuba: significance for Neogene–Quaternary tectonics of the Caribbean realm. Tectonophysics 396 (3–4), 161–180. https://doi.org/10.1016/j.tecto.2004.11.006.

Rojas-Agramonte, Y., Neubauer, F., Bojar, A.V., Hejl, E., Handler, R., Delgado, D.E.G., 2006. Geology, age and tectonic evolution of the Sierra Maestra Mountains, southeastern Cuba. Geol. Acta 123. https://raco.cat/index.php/GeologicaActa/article/view/82394.

Rosencrantz, E., 1990. Structure and tectonics of the Yucatan Basin, Caribbean Sea, as determined from seismic reflection studies. Tectonics 9 (5), 1037–1059. https://doi.org/10.1029/TC009i005p01037.

Rovere, A., Raymo, M.E., Vacchi, M., Lorscheid, T., Stocchi, P., Gomez-Pujol, L., Hearty, P.J., 2016. The analysis of last Interglacial (MIS 5e) relative sea-level indicators: reconstructing sea-level in a warmer world. Earth Sci. Rev. 159, 404–427. https://doi.org/10.1016/j.earscirev.2016.06.006.

Rovere, A., Ryan, D.D., Vacchi, M., Dutton, A., Simms, A.R., Murray-Wallace, C.V., 2022. The world atlas of last interglacial shorelines (version 1.0). Earth Syst. Sci. Data Discuss. 2022, 1–37.

Stirling, C.H., Esat, T.M., Lambeck, K., McCulloch, M.T., 1998. Timing and duration of the Last Interglacial: evidence for a restricted interval of widespread coral reef growth. Earth and Planet. Sci. Lett. 160 (3–4), 745–762.

Symithe, S., Calais, E., De Chabalier, J.B., Robertson, R., Higgins, M., 2015. Current block motions and strain accumulation on active faults in the Caribbean. J. Geophys. Res. Solid Earth 120 (5), 3748–3774. https://doi.org/10.1002/2014JB011779.

Taber, S., 1934. Sierra Maestra of Cuba, part of the northern rim of the Bartlett Trough. Bull. Geol. Soc. Am. 45 (4), 567–620. https://doi.org/10.1130/GSAB-45-567.

Thompson, W.G., Spiegelman, M.W., Goldstein, S.L., Speed, R.C., 2003. An open-system model for U-series age determinations of fossil corals. Earth Planet. Sci. Lett. 210 (1–2), 365–381. https://doi.org/10.1016/S0012-821X(03)00121–3.

Thurber, D.L., Broecker, W.S., Blanchard, R.L., Potratz, H.A., 1965. Uranium-series ages of Pacific atoll coral. Science 149 (3679), 55–58.

Toscano, M.A., Rodriguez, E., Lundberg, J., 1999. Geologic Investigation of the Late Pleistocene Jaimanitas Formation: Science and Society in Castro's Cuba.

Vaughan, T.W., Spencer, A.C., 1902. The geography of Cuba. Bull. Am. Geogr. Soc. 34 (2), 105–116. https://doi.org/10.2307/197566.

Vázquez-Taset, Y.M., Sàbat, F., Cabello, P., Cruz-Orosa, I., Ramos, E., 2020. Cenozoic tectonostratigraphic evolution of the strike-slip Cauto-Guacanayabo Basin, Eastern Cuba. J. S. Am. Earth Sci. 100, 102592. https://doi.org/10.1016/j.jsames.2020.102592.

Viruete, J.E., Pérez, Y., 2020. Neotectonic structures and stress fields associated with oblique collision and forearc sliver 1 formation in northern Hispaniola: implications for the seismic hazard assessment 2. Tectonophysics 784, 228452.

Weiss, T.L., Linsley, B.K., Gordon, A.L., Rosenthal, Y., Dannenmann-Di Palma, S., 2022. Constraints on marine isotope stage 3 and 5 sea level from the flooding history of the Karimata Strait in Indonesia. Paleoceanogr. Paleoclimatol. 37 (9), e2021PA004361. https://doi.org/10.1029/2021PA004361.

Wessels, R.J., 2019. Strike-slip fault systems along the northern Caribbean plate boundary. In: Transform Plate Boundaries and Fracture Zones. Elsevier, pp. 375–395. https://doi.org/10.1016/B978–0–12-812064-4.00015-3.

Ten Brink, U., Lin, J., 2004. Stress interaction between subduction earthquakes and forearc strike-slip faults: Modeling and application to the northern Caribbean plate boundary. J. Geophys. Res. Solid Earth 109 (B12).